

Florida State University Libraries

Electronic Theses, Treatises and Dissertations

The Graduate School

2010

Transport of Anthropogenic Emissions during ARCTAS-A: A Climatology and Regional Case Studies

Donal L. Harrigan



THE FLORIDA STATE UNIVERSITY
COLLEGE OF ARTS AND SCIENCES

TRANSPORT OF ANTHROPOGENIC EMISSIONS DURING ARCTAS-A: A
CLIMATOLOGY AND REGIONAL CASE STUDIES

By

DONAL L. HARRIGAN

A Thesis submitted to the
Department of Earth, Ocean & Atmospheric Science
in partial fulfillment of the
requirements for the degree of
Master of Science

Degree Awarded:
Fall Semester, 2010

The members of the committee approve the Thesis of Donal Harrigan defended on September 30, 2010.

Henry E. Fuelberg
Professor Directing Thesis

Guosheng Liu
Committee Member

Robert Hart
Committee Member

The Graduate School has verified and approved the above-named committee members.

AKNOWLEDGEMENTS

First, I would like to thank my major professor Dr. Henry Fuelberg for not only putting the bug in my ear to further my education by attending graduate school, but for also taking me on as a research assistant when I was far from a first round draft pick. His high standards and attention to detail were an integral part in the successful completion of this work.

This thesis, simply, would not have been possible without the efforts of Dr. Isobel Simpson from the chemistry department at the University of California-Irvine. Through countless emails, several phone chats, and multiple drafts of this work, she demonstrated a high level of patience while taking me through a crash course in atmospheric chemistry. Her contribution was crucial to the strong conclusions drawn from this study. It has been nothing short of a pleasurable experience working with her.

Thanks are also in order for my committee members Drs. Robert Hart and Guosheng Liu for their efforts to assure this thesis lived up to the standards of the Meteorology department.

I would like to thank my parents who continuously threw money into a black hole that seems to have finally closed. Without their support and guidance I don't see how any of this could have been possible. They helped mold me into the successful person that I am today. I should also thank my brother who unknowingly allowed me to spend most of his college fund on my surfing lessons in Melbourne, FL. My fiancée had to deal with grumpy Donal through the last couple of year and for that she is appreciated. I think we both look forward to a happier, less stressed version of me.

This research was sponsored by the NASA Tropospheric Chemistry Program under Grant NNX0AH72G.

TABLE OF CONTENTS

List of Tables	v
List of Figures	vi
Abstract	viii
1. INTRODUCTION	1
2. DATA AND METHODOLOGY	4
2.1 WRF Model	4
2.2 Trajectory Calculations	4
2.3 Chemical Data	7
3. RESULTS	10
3.1 Climatological Considerations	10
3.2 Eastern Asian Transport during ARCTAS-A	11
3.3 Eastern Asian Case Study	13
3.3.1 Chemical Fingerprinting	13
3.3.2 Transport and Meteorology	17
3.4 North American Transport during ARCTAS-A	23
3.5 North American Case Study	25
3.5.1 Chemical Fingerprinting	25
3.5.2 Transport and Meteorology	29
3.6 European Transport during ARCTAS-A	33
3.7 European Case Study	35
3.7.1 Chemical Fingerprinting	35
3.7.2 Transport and Meteorology	38
4. SUMMARY AND CONCLUSIONS	43
REFERENCES	46
BIOGRAPHICAL SKETCH	52

LIST OF TABLES

Table 1. WRF physics options used in this study. See Skamarock et al. (2008) for details about each option.	5
Table 2. Atmospheric lifetime, analytical details, and measurement statistics for selected compounds measured in the Asian plume. ARCTAS-A background averages also are included (see text for details).....	16
Table 3. As in Table 2, but for the North American plume.	28
Table 4. As in Table 2, but for the European plume.....	37

LIST OF FIGURES

Figure 1. Parent domain (45 km, black) and inner nests (15 km and 5 km, red) used for the ARCTAS simulations	5
Figure 2. The blue dots represent trajectory release locations on the $2.0^{\circ} \times 2.0^{\circ}$ grid for a) Asia, c) North America, and e) Europe. These locations were based on anthropogenic emissions during ARCTAS ($\text{kg grid point}^{-1} \text{ day}^{-1}$) for b) Asia, d) North America, and f) Europe from the CGRER data set	6
Figure 3. DC-8 flight tracks for a) Flight 5 on 5 April 2008, and b) Flight 8 on 12 April 2008. Trajectories were released at 1 min intervals along the segments shaded red.....	8
Figure 4. Trajectory statistics for the eastern Asia domain. a) Number and originating locations of trajectories reaching the Arctic (70°N). b) Pathways taken by all 15 day trajectories reaching the Arctic. c) Number and location of trajectories entering the Arctic. d) Pressure level at which Arctic bound trajectories arrive at 70°N	12
Figure 5. Vertical distribution plots for data from flight 8 on 12 April 2008 for a) 1,2-DCE, b) CH_3Cl , c) H-1211, d) OCS, e) C_2Cl_4 , and f) HCFC-22. Red points are data from leg 5. Blue points also are from leg 5 but represent the sampled plume. Black points represent the remaining legs of flight 8	15
Figure 6. Fifteen day backward trajectories for a) all trajectories associated with leg 5 that encountered the boundary layer sometime during their 15 day transit, b) only those segments of trajectories in (a) when the boundary layer is experienced, and c) pressure vs. time plot for trajectories from leg 5 that encountered the boundary layer.....	18
Figure 7. Conveyor belts associated with mid-latitude cyclones. (Adapted from the UCAR/COMET web site http://www.meted.ucar.edu/mesoprim/bandedprecip/print.htm#3.3)	19
Figure 8. Red circles denote the average location of trajectories comprising the easternmost branch in Fig. 7a for a) 9-10 days back from the flight, b) 6-7 days back, c) 5-6 days back, d) 4-5 days back, e) 2-3 days back, f) 1-2 days back.	21
Figure 9. Red circles denote the average location of trajectories comprising the westernmost branch in Fig. 7a for a) 10-15 days back from the flight, b) 6-7 days back, c) 4-5 days back, d) 3-4 days back.....	23
Figure 10. As in Fig. 4, but for North American trajectories.....	24

Figure 11. Vertical distribution plots for data from flight 5 on 5 April 2008 for a) C_2H_6 , b) C_3H_8 , c) C_6H_6 , d) HCFC-22, and e) C_2Cl_4 . Blue points are from leg 8, representing the sampled plume. In this case the plume is represented by all of the data points along leg 8. Black points represent the remaining legs of flight 5.	26
Figure 12. As in Fig. 6, but for leg 8 on 5 April 2008	30
Figure 13. Average positions of the group of trajectories released from leg 8 of the DC-8 flight on 5 April 2008. Red circles denote locations at a) 6-7 days back from the flight, b) 5-6 days back, c) 4-5 days back, and d) 3-4 days back.	32
Figure 14. As in Fig. 4, but for trajectories released from areas of European anthropogenic emissions	34
Figure 15. Vertical distribution plots for data from flight 8 on 12 April 2008 for a) C_2Cl_4 , b) C_2H_2 , c) C_6H_6 , d) CH_4 , e) C_2H_6 , and f) C_3H_8 . Red points are data from leg 8. Blue points also are from leg 8 but represent the sampled plume. Black points represent the remaining legs of flight 8.	36
Figure 16. As in Fig. 6, but for leg 8 on 12 April 2008	39
Figure 17. Trajectories as in Fig. 18a plotted with FLAMBE data (blue dots) for the period 26 March - 6 April 2008.	40
Figure 18. Red circles denote the average location of trajectories comprising the largest group of trajectories in Fig. 18a for a) 14-15 days back from the flight, b) 13-14 days back, c) 12-13 days back, d) 11-12 days back, e) 8-9 days back, and f) 7-8 days back.	42

ABSTRACT

The National Aeronautics and Space Administration (NASA) conducted the Arctic Research of the Composition of the Troposphere from Aircraft and Satellites (ARCTAS) mission during 2008 as a part of the International Polar Year (IPY). The purpose of ARCTAS was to study the factors responsible for changes in the Arctic's atmospheric composition and climate. A major emphasis was to investigate Arctic haze that is most pronounced during winter and early spring. This study focuses on the spring phase of ARCTAS (ARCTAS-A) that was based in Alaska during April 2008. Although anthropogenic emissions historically have been associated with Arctic haze, biomass burning dominated the ARCTAS-A period and has been the focus of many ARCTAS related studies.

This study determines the common pathways for anthropogenic emissions during ARCTAS-A. Trajectories are released each day from three historically significant regions of anthropogenic emissions (Asia, North America, and Europe). These fifteen day forward trajectories are calculated using data from the Weather Research and Forecasting (WRF) model at 45 km horizontal resolution. The trajectories then are examined to determine: Origins of emissions that reach the Arctic (defined as 70°N), pathways of the emissions reaching the Arctic, Arctic entry locations, and altitudes at which the trajectories enter the Arctic. These results serve as regional “climatologies” for the ARCTAS-A period.

Three cases during the ARCTAS-A period (one for each of the regions above) are examined using backward trajectories and chemical fingerprinting based on in situ data sampled by the NASA DC-8. The fingerprinting utilizes volatile organic compounds that represent pure anthropogenic tracers, Asian anthropogenic pollution, incomplete combustion, and natural gas emissions. We determine flight legs containing anthropogenic emissions and the pathways travelled by these emissions. Results show that the DC-8 sampled anthropogenic emissions from Asia, North America, and Europe during the spring phase of ARCTAS. The pathways travelled by these emissions agree with our derived “climatologies” and previous studies of Arctic transport. Meteorological analysis and trajectory calculations indicate that middle latitude cyclones and their associated warm conveyor belts play an important role in lofting the surface based emissions to their sampling altitude in all three cases.

CHAPTER 1

INTRODUCTION

Since the Arctic is far removed from most industrial locations and other sources of pollution, its atmosphere long was believed to be very clean (Stohl, 2006; Law and Stohl, 2007). However, parts of the Arctic actually can become very polluted due to the transport of emissions from distant sources (Raatz and Shaw, 1984; Shaw, 1995; Rinke et al., 2004). The greatest concentrations of Arctic pollution occur during the winter and early spring months (Mitchell, 1957; Shaw, 1995; Eckhardt et al., 2003). The buildup of pollutants during these months, combined with photochemical reactions (beginning in early spring), produce a visibility reducing haze called “Arctic Haze” (Mitchell, 1957; Shaw, 1982; Hileman, 1983; Schnell, 1984; Meyer et al., 1990). This phenomenon first was documented during the 1950’s by air force pilots during weather reconnaissance flights (Mitchell, 1957). The haze typically is most concentrated near the surface, with discontinuous horizontal layers in the middle and upper troposphere (Hileman, 1983; Hoff, 1987).

Arctic haze long was considered to consist mostly of anthropogenic pollutants (Hileman, 1983; Barrie and Hoff, 1985; Barrie et al., 1994; Stohl, 2006; Warneke et al., 2009), with primary species being a mixture of sulphates and particulate organic matter (Li and Barrie, 1993; Quinn et al. 2002). Other species include ammonium, nitrate, dust and black carbon (Li and Barrie, 1993; Quinn et al., 2002). Shaw (1995) noted that heavy metals detected in the haze are associated with industrial sources. Recent research has shown that boreal forest fires in Siberia and eastern China, as well as agricultural burning in Kazakhstan, southern Russia, and eastern Europe also are important sources of Arctic pollution (Warneke et al., 2009; Warneke et al., 2010). This source of biomass emissions may increase in the future due to the effects of climate change (Kasischke et al., 2005).

Several factors contribute to the buildup of pollutants in the Arctic atmosphere. First, the Arctic atmosphere is dominated by strong temperature inversions that trap air near the surface, especially during the winter and early spring when there is little or no sunlight (Curry, 1983, 1987; Raatz, 1991; Bradley et al., 1992). Since these inversions limit turbulent mixing, dry deposition also is greatly reduced (Hileman, 1983; Stohl and Law, 2006). Furthermore, since the

atmosphere during the winter and early spring is cold, dry, and stable, precipitating cloud systems are inhibited, thereby limiting wet deposition (Shaw, 1995). Another phenomenon that influences cold season Arctic transport is the “dome” of cold potential temperature that forms over the polar region (Klonecki et al., 2003; Stohl, 2006; Law and Stohl, 2007). Since potential temperature increases with altitude in the stable atmosphere, and due to the temperature difference between the middle latitudes and the Arctic, the potential temperature (isentropic) surfaces curve upward from the mid latitudes to the Arctic (Carlson, 1981; Iverson, 1984; Raatz, 1991). If one assumes adiabatic conditions, low level air parcels moving northward from the middle latitudes must ascend as they approach the Arctic. Conversely, for parcels to remain near the surface, they must be diabatically cooled by radiative effects or other processes during passage over the ice covered surfaces.

Three typical transport pathways to the Arctic during the winter months have been identified by Stohl (2006) and Stohl and Law (2006). The first consists of rapid low level transport of already cold air north of the Arctic Front. A variation of this scenario is rapid transport of air that is lifted over the Arctic Front. The second method of transport occurs on a longer time scale in which cold air is transported over a snow covered surface, allowing it to cool sufficiently to penetrate the Arctic isentropic dome. Finally, middle latitude air can be lofted into the upper troposphere and then quickly transported to the Arctic where it gradually sinks into the lower troposphere due to radiative cooling. These three transport processes generally mean that European emissions are the dominant source of pollutants in the low levels of the Arctic, while North American and east Asian pollutants are more common in the middle and upper levels (Klonecki et al., 2003; Stohl, 2006; Law and Stohl, 2007).

The National Aeronautics and Space Administration (NASA) conducted the Arctic Research of the Composition of the Troposphere from Aircraft and Satellites (ARCTAS) field mission during 2008 (Jacob et al., 2010). ARCTAS was conducted primarily over the Arctic areas of Canada and Greenland. Its European counterpart was the Polar Study using Aircraft, Remote Sensing, Surface Measurements and Models of Climate, Chemistry, Aerosols and Transport (POLARCAT, Stohl and Law, 2006) study spanning the International Polar Year (IPY). ARCTAS consisted of two deployments, one based in Alaska (April 2008) and the other in Alberta, Canada (June-July 2008) (Jacob et al., 2010). The main goal of ARCTAS was to better understand the factors that contribute to changes in the composition of the Arctic

atmosphere and climate by studying the influx of mid-latitude pollutants, boreal forest fire emissions, aerosol radiative forcing, and chemical processes (Jacob et al., 2010).

Anthropogenic emissions were expected to dominate the Arctic atmosphere during the spring phase of ARCTAS (hereafter denoted ARCTAS-A). However, that did not occur. Instead, widespread fires in Russia were the major source of Arctic pollution at that time (Warneke et al., 2009; Jacob et al., 2010). The fires started unusually early, consisting of agricultural burning in Kazakhstan and southern Russia as well as boreal forest fires in Siberia (Warneke et al., 2009). ARCTAS related research has examined the sources and characteristics of the biomass emissions (i.e., Singh et al., 2010; Oltmans et al., 2010; Matsui et al., 2010). Although biomass burning emissions were the dominant source of Arctic pollution during ARCTAS-A, our focus is the characteristics and transport pathways of anthropogenic emissions during the spring period, specifically the influx of mid-latitude anthropogenic pollutants to the Arctic and how the transport pathways during the spring (April) phase of ARCTAS compare with those previously described in the literature. We utilize in situ chemical data sampled by the NASA DC-8 flying laboratory and backward kinematic trajectories derived from high resolution numerical modeling to identify source regions of the anthropogenic emissions that were sampled by the aircraft. Three specific cases are examined, one for each of the major source regions, Europe, Asia, and North America. These cases are compared to transport occurring during the entire spring phase of ARCTAS.

Section 2 provides details about the meteorological numerical model that we employed as well as the trajectory products derived from its output. Information about other methodologies and the specifics of our various data sources also is provided. Section 3 presents derived ARCTAS-A “climatologies” for each of the three major source regions as well as results from the three cases of anthropogenic Arctic transport. The final section summarizes our findings and presents conclusions.

CHAPTER 2

DATA AND METHODOLOGY

2.1 WRF Model

Numerical simulations were used to study weather patterns responsible for transport to the Arctic (defined as the region north of 70°N) during the ARCTAS mission. This study utilized the Weather Research and Forecast (WRF) model (Skamarock et al., 2008) version 3.0.1.1 developed by the National Center for Atmospheric Research (NCAR). The parent domain had a 45 km horizontal resolution centered on the North Pole (Fig. 1). Inner telescoping nests of 15 and 5 km were centered over three historically significant anthropogenic source regions including Europe, eastern Asia, and North America. These inner nests provided two-way feedback to the coarse grid. The parent domain and each of the inner nests utilized a polar stereographic projection and consisted of 50 vertical sigma levels that were packed in the boundary layer and near the tropopause. The specific physics packages used in our WRF simulations are listed in Table 1 and Fuelberg et al. (2010). In depth discussions about each of the settings in Table 1 can be found in Skamarock et al. (2008). The model was initialized with final analysis data from the Global Forecast System (GFS) at 0.5°× 0.5° horizontal resolution. GFS is run operationally by the National Center for Environmental Prediction (available at <http://www.nco.ncep.noaa.gov/pmb/products/>, 2007).

2.2 Trajectory Calculations

Trajectories were calculated using hourly wind data from the WRF 45 km grid. Specific information on the trajectory model can be found in Fuelberg et al. (1996, 2000) and Martin et al. (2002). Limitations of trajectories are described in Stohl et al. (1995), Stohl et al. (1998), and Fuelberg et al. (2000). We used trajectories to (1) derive general transport statistics for the three regions of interest (Europe, Asia, and North America) during the entire spring phase of ARCTAS, and (2) to study transport during three specific case studies (one for each region listed above).

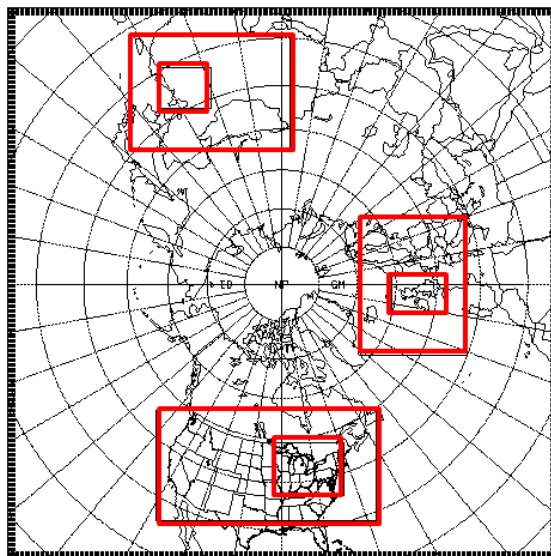


Fig. 1. Parent domain (45 km, black) and inner nests (15 km and 5 km, red) used for the ARCTAS simulations.

Table 1. WRF physics options used in this study. See Skamarock et al. (2008) for details about each option.

Option	Setting
Microphysics	Morrison Double-Moment
Longwave Radiation	Rapid Radiative Transfer Model
Shortwave Radiation	Goddard
Surface Layer	ETA Similarity
Land Surface	NOAH
Boundary Layer	Mellor-Yamada-Janjic
Cumulus Parameterization	Kain-Fritsch

Anthropogenic CO emissions data from the University of Iowa Center for Global and Regional Environmental Research (CGRER) were used to define trajectory “release” locations in regions of emissions (Fig. 2). These data had been prepared to support the ARCTAS mission (for further information and data access, see <http://www.cgrer.uiowa.edu/arctas/emission.html>). To derive general transport statistics during ARCTAS-A, fifteen day forward trajectories were released at the surface on a $2.0^\circ \times 2.0^\circ$ grid within the domains of each of our areas of interest. Releases were made each day (~ 2 PM LDT) during the period 19 March through 17 April 2008, with data for the final day of trajectories extending to 3 May 2008.

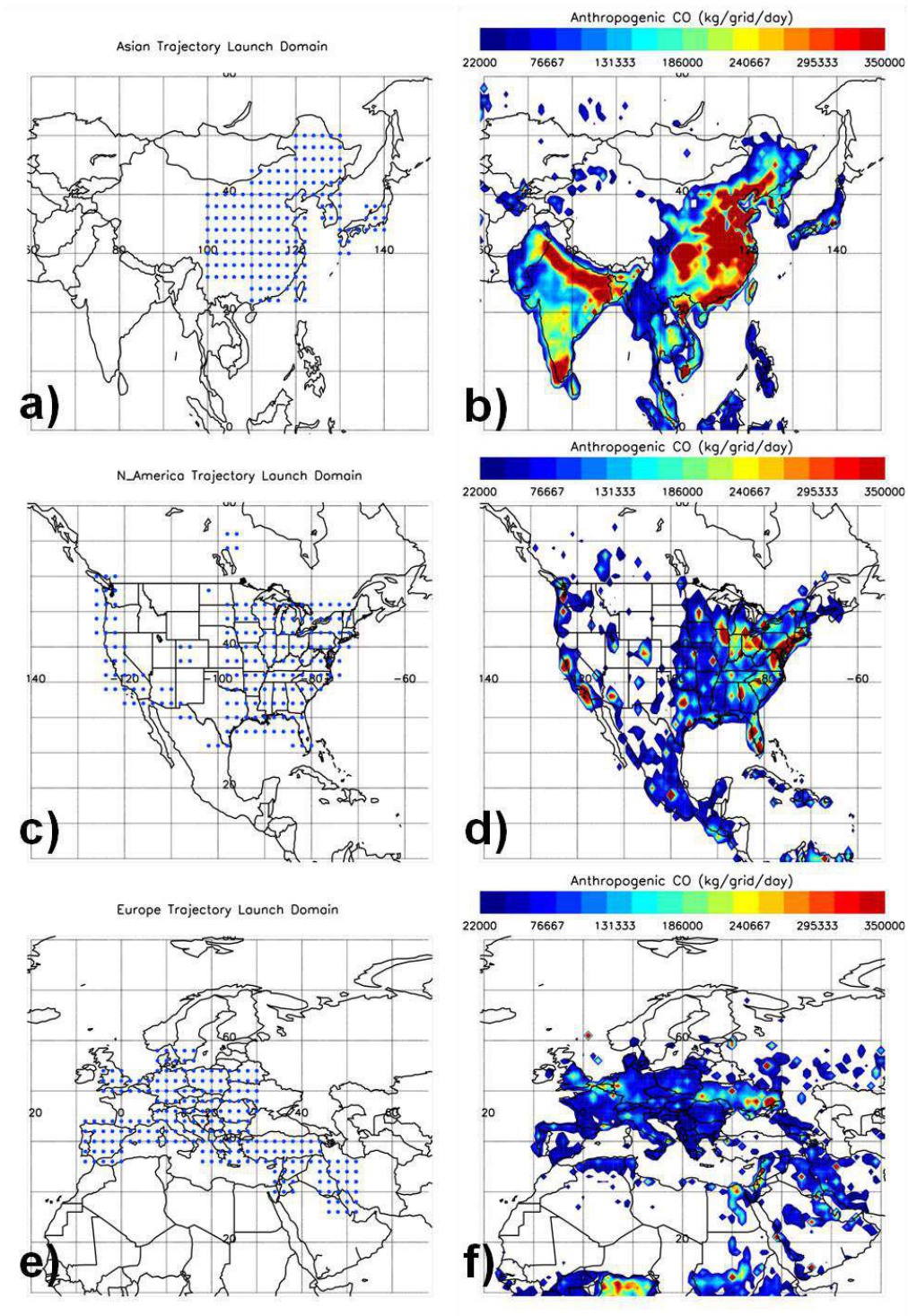


Fig. 2. The blue dots represent trajectory release locations on the $2.0^\circ \times 2.0^\circ$ grid for a) Asia, c) North America, and e) Europe. These locations were based on anthropogenic emissions during ARCTAS ($\text{kg grid point}^{-1} \text{ day}^{-1}$) for b) Asia, d) North America, and f) Europe from the CGRER data set.

Trajectories for the three case studies were calculated using the same trajectory model described above and using the same WRF-derived wind data. These trajectories extended 15 days backward in time and were released at 1 min intervals along specific legs of DC-8 flights 5 and 8 (Fig. 3).

2.3 Chemical Data

The University of California-Irvine (UCI) atmospheric chemistry group used whole air sampling (WAS) techniques to measure 76 speciated volatile organic compounds (VOCs) during each DC-8 flight of the ARCTAS campaign (Simpson et al., 2010). We used these data to identify anthropogenic emissions and tag their respective source regions. In particular we used carbonyl sulphide (OCS), halon-1211 (H-1211), methyl chloride (CH_3Cl) and 1,2-dichlorethene (1,2-DCE) as tracers of Asian anthropogenic pollution plumes (Barletta et al., 2009); ethyne (C_2H_2) and benzene (C_6H_6) as tracers of incomplete combustion, including biomass burning and/or urban fossil fuel (Blake et al., 2003; Warneke et al., 2007); methane (CH_4), ethane (C_2H_6) and propane (C_3H_8) as probes for natural gas (Katzenstein et al., 2003; Xiao et al., 2008); and tetrachloroethene (C_2Cl_4) and HCFC-22 as purely anthropogenic tracers since they have no known natural sources (Aucott et al., 1999; Simpson et al., 2004). Specific information about the sampling techniques and processing of these data can be found in Blake (2008), Simpson et al. (2010), and the references therein. Briefly, 168 whole air canisters were loaded on the DC-8 prior to each flight, and were filled sequentially throughout the flight. Sampling times typically were 1 min during horizontal flight legs, and 30 s to 1 min during ascents and descents. Because of the finite number of canisters, samples generally were taken every 4-5 min, and more frequently during ascents, descents, and plume encounters. The detection limit, precision and accuracy of the measurements vary by compound, and are shown for the 10 species that we considered in Tables 2, 3, and 4 of the results section. These 10 compounds have a range of atmospheric lifetimes, from 9 days (benzene) to 16 years (H-1211) (Tables 2, 3, and 4). Trace gases undergo chemistry and mixing as soon as they are released from their emission source, and a short-lived gas such as benzene will become relatively more depleted during its multi-day transit from its emission source to the DC-8 sampling location. Therefore, our identification of anthropogenic plumes from specific emission source regions was based on a combination of chemical fingerprinting and back trajectory analysis, rather than by

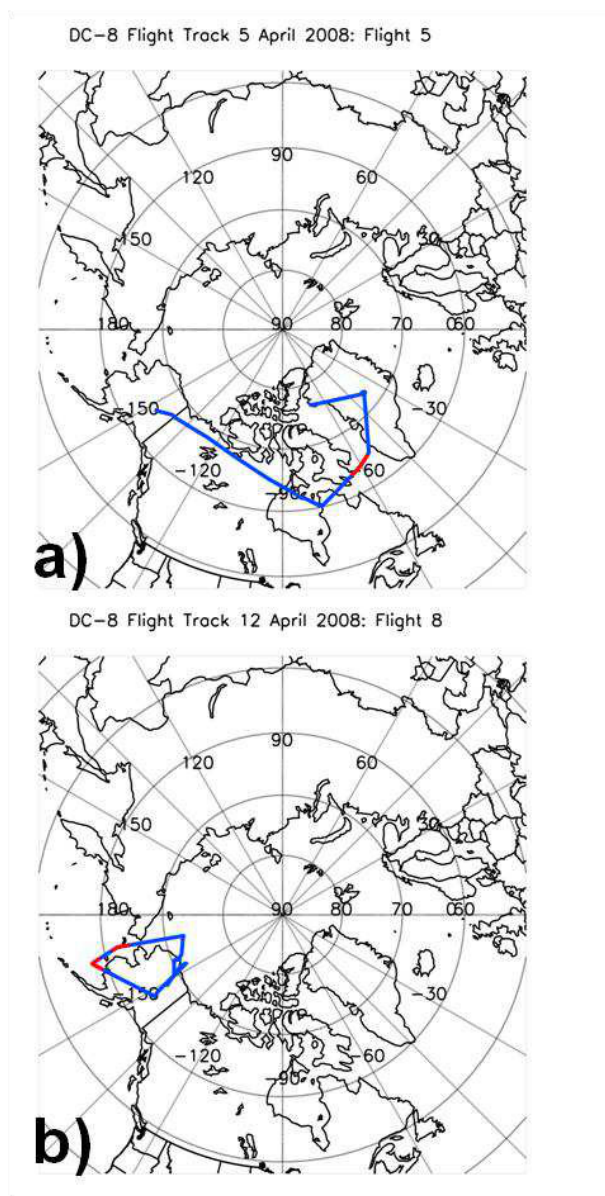


Fig. 3. DC-8 flight tracks for a) Flight 5 on 5 April 2008, and b) Flight 8 on 12 April 2008. Trajectories were released at 1 min intervals along the segments shaded red.

attempting to compare the measured data to known emission ratios from specific sources, which requires relatively fresh plumes to be sampled (minutes to hours old).

An additional consideration in the analysis is that many of the trace gases being examined vary with time (diurnally, seasonally, and annually) and space (latitudinally and altitudinally). For example HCFC-22 is experiencing rapid year-to-year growth (Montzka et al., 2009), whereas global C_2Cl_4 levels are continuing a long-term decline (Simpson et al., 2004).

Therefore, we calculated a local background for each compound that is appropriate for the season and latitudes that were sampled during ARCTAS-A. Specifically, data from flights 4-10 were used (this excludes flights 3 and 11, which were transit flights between Palmdale, CA and Fairbanks, AK). Stratospheric data were removed by choosing a cutoff of $O_3 > 100$ ppbv. Furthermore, O_3 depletion episodes at low altitudes were removed by choosing a cutoff of $O_3 < 45$ ppbv. This removed 338 of 1126 data points, leaving 788 points. The background average for each compound then was calculated using the lowest quartile (25%) of the remaining data ($n = 197$). These local background averages were compared to the plume enhancements.

CHAPTER 3

RESULTS

3.1 Climatological Considerations

Before discussing common transport pathways during ARCTAS-A, and the meteorology responsible for this transport, it is important to briefly discuss the climatology of the northern hemispheric spring season during ARCTAS-A and how it differed from typical conditions. Fuelberg et al. (2010) compared ARCTAS-A time-averaged positions of surface, middle, and upper level features with climatological averages. A summary of their results follows.

At the surface, the Pacific subtropical high was slightly stronger than average, extending further north than usual (Fuelberg et al., 2010). As a result, the “Aleutian Storm Track” was displaced north of its climatological position. Although the Siberian and Polar highs were near their climatological positions, the Siberian high had below average pressures along its eastern periphery, while the Polar high was slightly stronger than average. The “Atlantic Storm Track” was weaker than average across the western reaches of the Atlantic, while enhanced cyclonic activity occurred over the eastern Atlantic, probably because the subtropical Atlantic high did not extend as far east as is typical.

In the middle levels, higher than average geopotential heights were located across the northern Pacific, northwestern Atlantic, Greenland, and northwestern Russia (Fuelberg et al., 2010). Conversely, lower than average heights extended across the eastern Atlantic, Siberia, western Canada, and the northwestern United States. In the upper levels, the polar jet stream over the northeastern Pacific was positioned farther north than average. Westerly flow over the north Atlantic generally was enhanced, except over the north central Atlantic just east of Greenland.

Forward trajectories were analyzed by Fuelberg et al. (2010) to determine the most common transport pathways during ARCTAS-A. We followed a similar approach but focused on the three primary anthropogenic source regions (Asia, North America, and Europe). The following sections begin with forward trajectory transport statistics for each of these regions, followed by a case study of each source region that employs chemical tracers and backward trajectories.

3.2 Eastern Asian Transport during ARCTAS-A

To identify the Arctic bound transport pathways specific to eastern Asia (as defined Fig. 2a), 15 day forward trajectories were calculated from the WRF model data. During the period 19 March through 17 April 2008, 173 trajectories were launched each day from the Asian domain (Fig. 2a), producing a total of 5363 releases during the 31 day period. After the trajectories were calculated, their information was combined to determine (1) how many trajectories (per domain grid point) reached the Arctic (crossed 70°N); (2) the common pathways taken by these trajectories; (3) common Arctic entry locations along the 70°N latitude belt; (4) and the pressure level at which the trajectories entered the Arctic.

Fig. 4a shows the origins of Asian trajectories that enter the Arctic during ARCTAS-A. In general, trajectories released further north have a greater chance of being transported to the Arctic, while some locations in the southern portion of the domain fail to produce an Arctic bound trajectory. Within the Asian domain, 40.2% of the 528 Arctic bound trajectories were released at a latitude greater than 40°N, 54.7% came from the region between 30°N and 40°N, and only 5.1% originated further south than 30°N.

To determine the pathways taken by trajectories crossing 70°N, the hourly position of each trajectory that reached the Arctic was plotted (Fig. 4b shows the results at 1° × 1° resolution). Once the trajectory entered the Arctic, it was no longer tracked. Although this plot shows trajectory counts at each grid point, it clearly depicts high traffic regions that can be interpreted as pathways. While most trajectories released from Asia travel eastward, one distinct pathway is evident. It extends across eastern Siberia and the North Pacific Ocean, over the Bering Sea, northward across western Alaska, and into the Arctic. Other “hot spots” are located across western Canada and the central United States.

The aforementioned primary pathway is reflected in the plot of Arctic entry locations (Fig. 4c), where each colored circle represents an entry region that is 5° longitude wide. If a trajectory exited the Arctic and subsequently re-entered, only the first entrance was recorded. The most common Arctic entry location from eastern Asia is along the extreme northeastern part of Siberia, eastward through the Chukchi Sea, and along northwestern and north-central Alaska. In fact, 61.5% of the trajectories that reach the Arctic enter between 180-140°W. Very few Asian trajectories enter the Arctic from the northeastern Atlantic Ocean and locations eastward through western and central Russia.

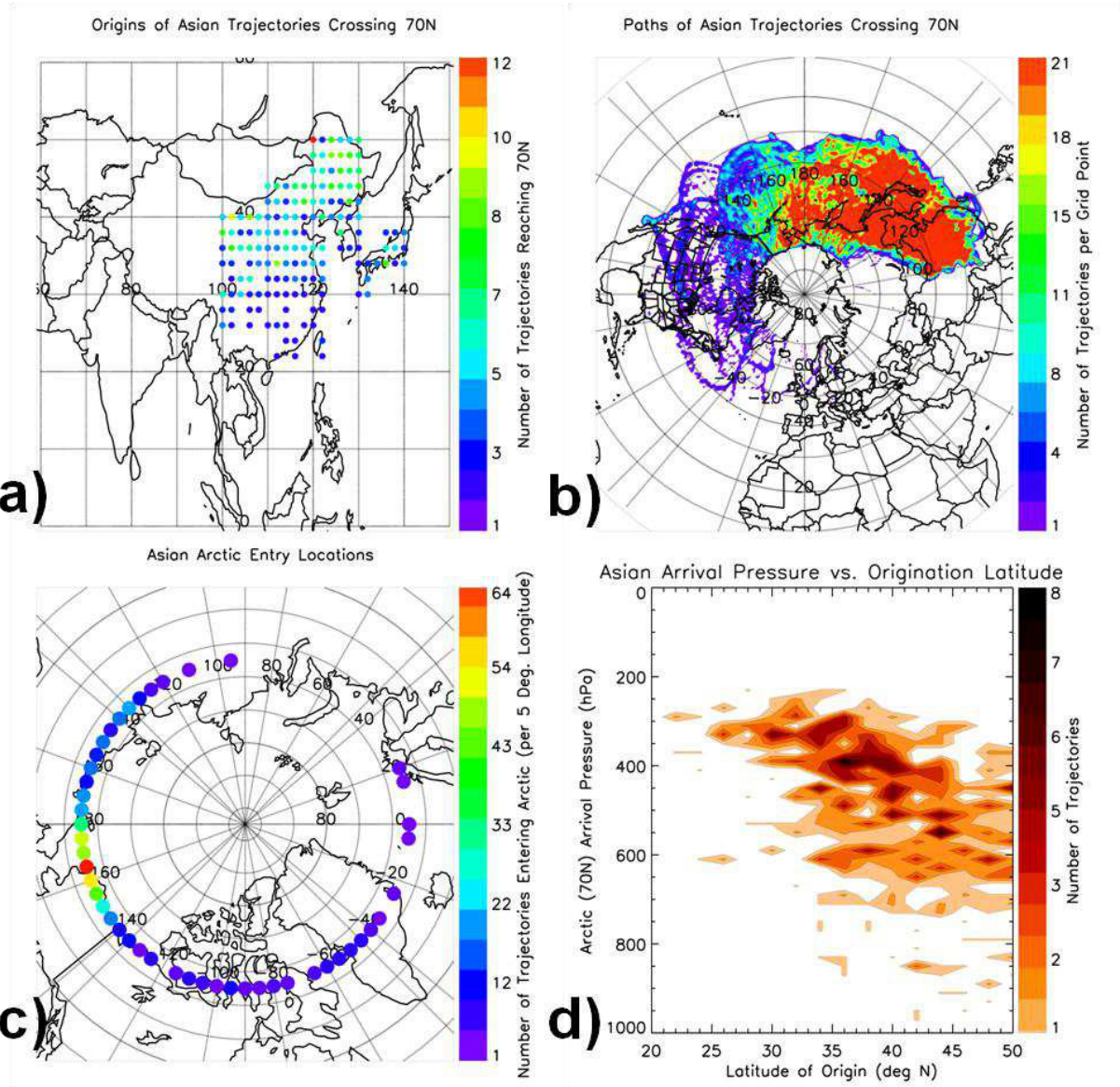


Fig. 4. Trajectory statistics for the eastern Asia domain. a) Number and originating locations of trajectories reaching the Arctic (70° N). b) Pathways taken by all 15 day trajectories reaching the Arctic. c) Number and location of trajectories entering the Arctic. d) Pressure level at which Arctic bound trajectories arrive at 70° N.

The most common Arctic arrival pressures for Asian trajectories are in the middle (850 – 500 hPa) and upper (less than 500 hPa) troposphere (Fig. 4d). Only 3.2% of the trajectories reaching the Arctic do so in the lower troposphere (greater than 850 hPa), while 40.5% arrive in the middle troposphere and 56.3% arrive in the upper troposphere.

3.3 Eastern Asian Case Study

We now present an example of Asian anthropogenic transport using chemical tracers sampled by the DC-8 and backward trajectories. We fingerprint the source region of the sampled anthropogenic emissions and describe its transport pathway and the weather patterns responsible for this transport. Asian emissions have been found to be more efficient in producing tropospheric ozone than European and North American sources (Stohl et al., 2002). Thus, understanding the pathways and receptor regions of Asian anthropogenic emissions is important in understanding atmospheric chemistry budgets.

Leg 5 of DC-8 flight 8 on 12 April 2008 is an example of transport from Asia to the Arctic. Flight legs were determined using standard techniques of the Florida State University (FSU) Meteorology group (more information can be found at <http://fuelberg.met.fsu.edu/research/arctas/traj/traj.html>). Leg 5 extends between 17:30 and 18:03 UTC, and is shown in Fig. 3b as the southernmost red segment, just south of Nunyak Island, AK.

3.3.1 Chemical Fingerprinting

Asian outflow consists of a complex mixture of industrial, biofuel, and biomass burning emissions (Russo et al., 2003; Streets et al., 2003). Distinguishing anthropogenic influences from biomass burning during ARCTAS-A is complex since the influence of biomass burning was significant. However, based on airborne measurements made during NASA's Intercontinental Chemical Transport Experiment (INTEX-B), Barletta et al. (2009) noted that China has a distinct anthropogenic chemical fingerprint consisting of enhanced carbonyl sulphide (OCS), methyl chloride (CH_3Cl), 1,2-dichloroethane (1,2-DCE), ethyl chloride, and halon-1211 (H-1211). The following description indicates that the ARCTAS flight 8, leg 5 chemical signature is consistent with that fingerprint.

Carbonyl sulphide has several sources, including oceans, biomass burning, aluminum production, and coal combustion (Watts, 2000; Kettle et al., 2002; Blake et al., 2004). Sources of CH_3Cl include biomass burning and biofuel use, while 1,2-dichloroethane primarily is anthropogenic and is used as a chemical intermediate in synthesizing other compounds (Barletta et al., 2009). Halon-1211, a purely anthropogenic tracer, is used in firefighting (Butler et al., 1998; Fraser et al., 1999). Halon-1211 also contributes to stratospheric ozone depletion,

although its global abundance has begun to decline in recent years (D. Blake, pers. comm., 2010; <http://cdiac.ornl.gov/trends/otheratg/blake/data.html>). Although CH₃Cl and OCS can have both anthropogenic and biomass burning sources, their origins can reasonably be classified as anthropogenic when well correlated with H-1211 and 1,2-DCE. These species, as well as tetrachloroethene (C₂Cl₄, an industrial solvent and purely anthropogenic tracer) and HCFC-22 (a refrigerant and purely anthropogenic tracer) (Aucott et al. 1999; Blake et al., 2003) are plotted in Fig. 5 with respect to sampling altitude along DC-8 flight 8 on 12 April 2008.

Sampling altitudes, as well as mixing ratios identify three data points between 7500-8300 m that represent the plume sampled along leg 5. Fig. 5 presents six composite plots with leg 5 indicated by the red points. The blue points also represent data from leg 5, specifically the subset of leg 5 data that represents the plume that will be examined. All other legs along flight 8 are represented by the black points.

Figs. 5a-d show the tracers described by Barletta et al. (2009) as being an anthropogenic fingerprint for China. It is clear that the data points representing the plume (blue) are enhanced over the background values for the flight. Furthermore, a relatively strong average correlation ($r^2 = 0.81$) between these four tracers supports the conclusion that OCS and CH₃Cl within the leg 5 plume are of anthropogenic origin. Further strengthening the theory that anthropogenic emissions were sampled along leg 5 is the fact that two purely anthropogenic tracers (C₂Cl₄ and HCFC-22, Figs. 5e, f) are enhanced over background values.

Mean background mixing ratios for each of the species above were determined using data from ARCTAS-A flights 4-10, as described in Section 2.3, and are presented in Table 2. These values are compared with mean mixing ratios in the plume along leg 5. All species listed in Table 2 show higher mixing ratios in the leg 5 Asian plume than in background air measured during ARCTAS-A. The mean values of 1,2-DCE, C₂Cl₄, CH₃Cl, OCS, HCFC-22, and H-1211 in the Asian plume are enhanced by 420, 61, 30, 26, 8 and 7%, respectively, over their mean background values (Table 2). One should note that these relative enhancements generally decrease with increasing atmospheric lifetime of each compound. This is consistent with longer-lived species being more abundant (higher background values) in the atmosphere, therefore producing relatively smaller enhancements.

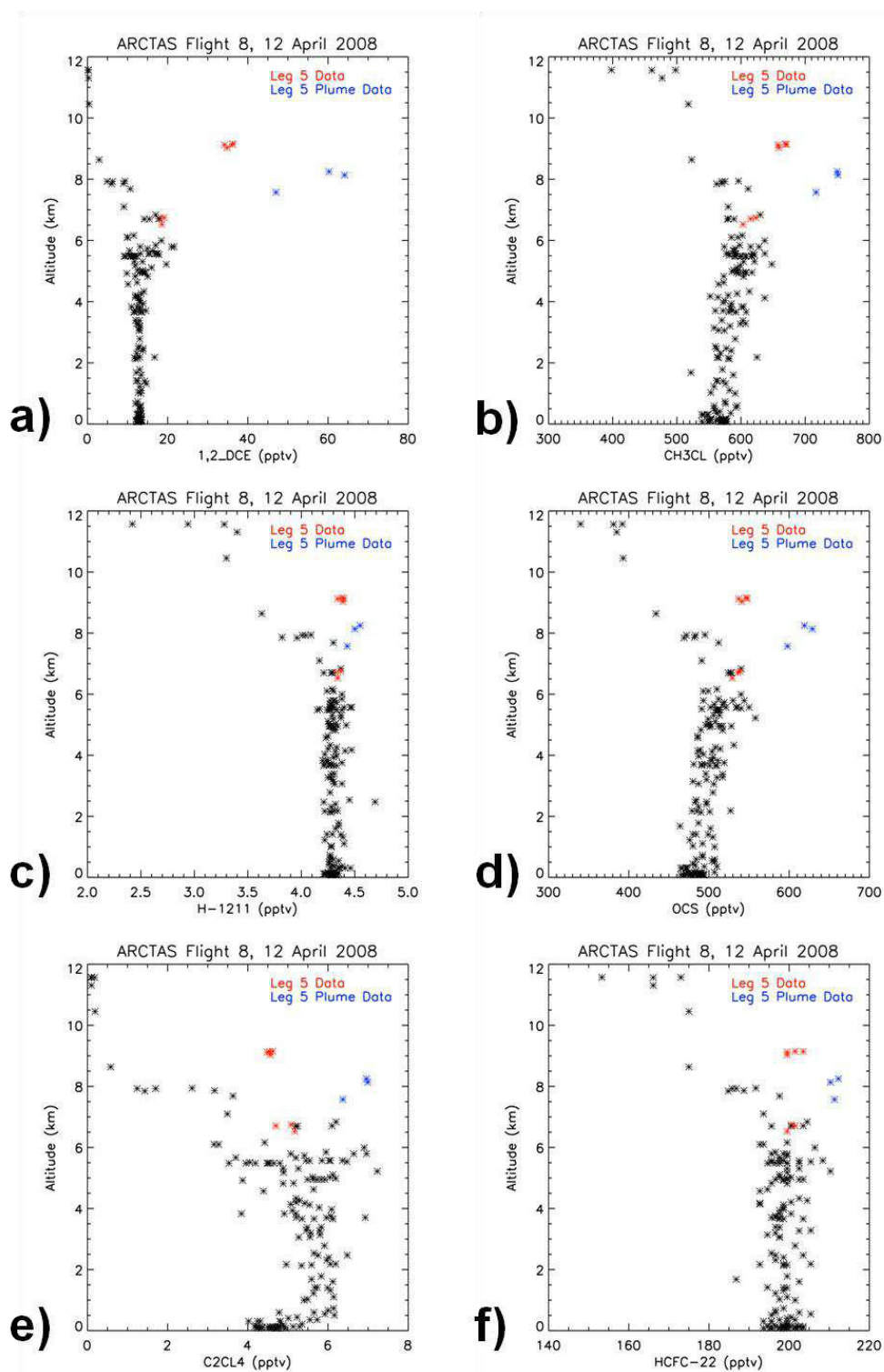


Fig. 5. Vertical distribution plots for data from flight 8 on 12 April 2008 for a) 1,2-DCE, b) CH₃Cl, c) H-1211, d) OCS, e) C₂Cl₄, and f) HCFC-22. Red points are data from leg 5. Blue points also are from leg 5 but represent the sampled plume. Black points represent the remaining legs of flight 8.

Table 2. Atmospheric lifetime, analytical details, and measurement statistics for selected compounds measured in the Asian plume. ARCTAS-A background averages also are included (see text for details).

Compound	Formula	Lifetime	LOD (pptv)	Precision (%)	Accuracy (%)	Bkgd. Avg. (pptv)	Bkgd. St. Dev. (pptv)	Asian Plume Avg. (pptv)	Asian Plume St. Dev. (pptv)	Enhancement over average background (%)	Asian Plume Max (pptv)
1,2-Dichloroethane	1,2-DCE	1-2 mo	0.1	5	10	11.0	0.8	57	9	420	64
Methyl chloride	CH ₃ Cl	1.0 yr	50	5	10	567	7	739	19	30	751
Halon-1211	H-1211	16 yr	0.10	1	5	4.20	0.04	4.49	0.06	7	4.55
Carbonyl sulphide	OCS	2.5 yr	10.00	2	10	487	4	615	16	26	629
Tetrachloroethene	C ₂ Cl ₄	2-3 mo	0.01	5	10	4.20	0.60	6.77	0.35	61	6.99
HCFC-22	HCFC-22	12 yr	2.00	5	5	195	2	211.3	1.0	8	212.3

To summarize, enhancements in three purely anthropogenic tracers (C_2Cl_4 , H-1211, and HCFC-22) signal an anthropogenic influence along leg 5 of flight 8 on 12 April 2008. Furthermore, four species known to be specific to Chinese anthropogenic emissions (1,2-DCE, OCS, H-1211, and CH_3Cl) are well correlated along leg 5. The two species that can have either biomass or anthropogenic emissions (OCS and CH_3Cl) are concluded to be of anthropogenic origins since they are well correlated with the remaining two anthropogenic tracers (H-1211 and 1,2-DCE). Furthermore, the anthropogenic signature along leg 5 is enhanced over all other flights during ARCTAS-A. Thus, based on chemistry alone, Chinese anthropogenic emissions were sampled along leg 5. This Chinese source is examined from a meteorological perspective in the next section.

3.3.2 Transport and Meteorology

Thirty-four 15 day backward trajectories were released at 1 min intervals along flight leg 5 within the 500-300 hPa layer. We monitored whether each trajectory passed into the model-derived boundary layer during its transit, and all 34 trajectories were found to have done so (Fig. 6a). Boundary layer encounters are important since they indicate that surface based emissions are accessed for transport. Working backward from the flight leg, the trajectories remain in the upper levels as they travel westward across the Bering Sea. As they reach the Sea of Okhotsk, they split into two segments. One segment travels due south of the Kamchatka Peninsula as it begins to descend. It travels south of Japan and South Korea before turning westward and passing onshore across eastern China. The other segment of trajectories continues west of the peninsula before descending over Japan. It then spirals left 270° over the northwestern Pacific Ocean before continuing in the lower levels west across Japan and eastern Asia.

Since we seek to confirm whether eastern Asia is the source of anthropogenic emissions during leg 5, it is important to know if the leg 5 trajectories pass through that region's boundary layer. Fig. 6b shows those segments of the trajectories in Fig. 6a that are in the boundary layer. Trajectories are in the boundary layer along the entire coast of eastern Asia, as well as over the northwestern Pacific Ocean, and off the eastern shore of Japan, where anthropogenic emissions are enhanced (Fig. 2b).

Fig. 6c presents the trajectories from Fig. 6a in a pressure versus time reference frame. Both branches of trajectories experience deep ascent beginning ~ 4 days prior to flight 8. The

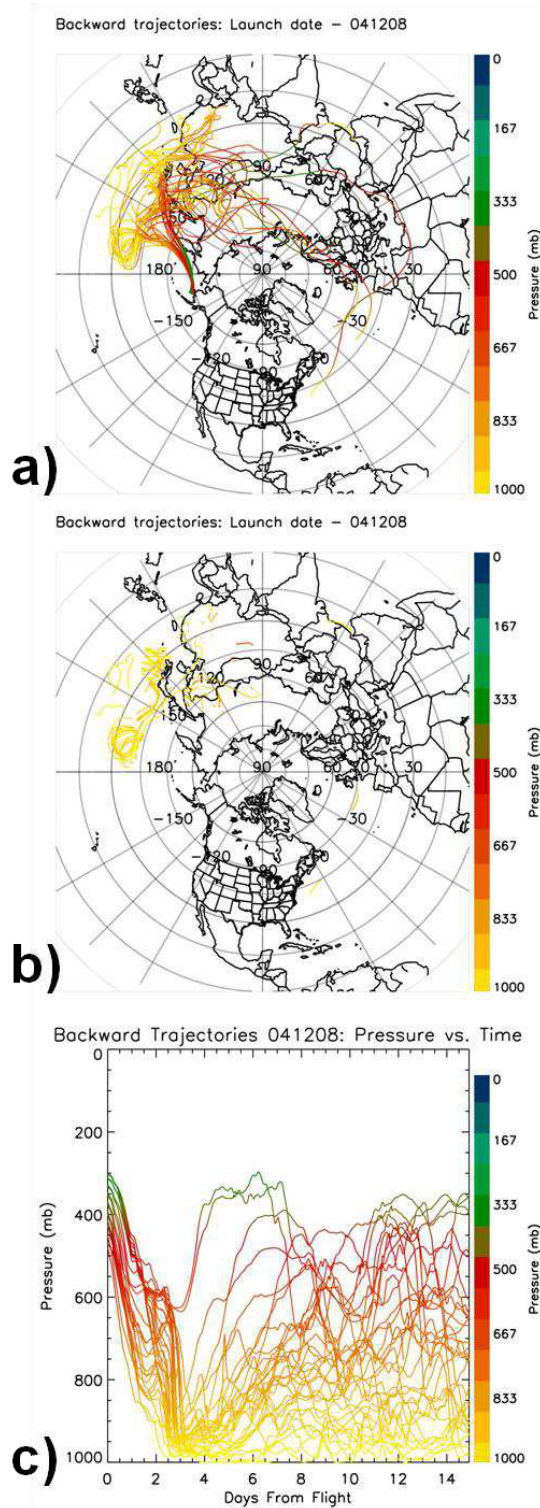


Fig. 6. Fifteen day backward trajectories for a) all trajectories associated with leg 5 that encountered the boundary layer sometime during their 15 day transit, b) only those segments of trajectories in (a) when the boundary layer is experienced, and c) pressure vs. time plot for trajectories from leg 5 that encountered the boundary layer.

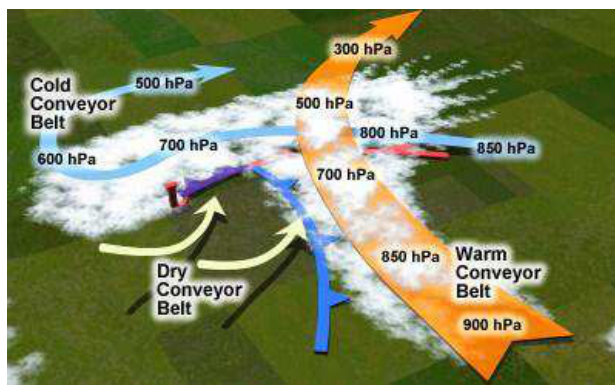


Fig. 7. Conveyor belts associated with mid-latitude cyclones. (Adapted from the UCAR/COMET web site <http://www.meted.ucar.edu/mesoprism/bandedprecip/print.htm#3.3>)

distribution on prior days is less defined due to the different paths taken by the individual trajectories. Synoptic analyses indicate that the strong ascent beginning at day 4 is due to a warm conveyor belt (WCB). A WCB is an airstream ahead of a surface cold front that originates near the surface of a cyclone's warm sector and then ascends to the upper troposphere (Eckhardt et al. 2004). Fig. 7 is a schematic of a WCB and other major airstreams in relation to their parent middle latitude cyclone. Warm conveyor belts play an integral role in transporting boundary layer air into the upper levels of the atmosphere where it can undergo subsequent long range transport (Ding et al., 2009). WCBs most commonly originate along the east coasts of North America and Asia and are more frequent during Northern Hemisphere winter than summer (Stohl, 2001; Eckhardt et al., 2004). Based on a 15 year climatology, Eckhardt et al. (2004) determined the timescale of WCBs to be ~ 2 days. They classified "reasonably strong" WCBs based on trajectories that during a 2 day time period ascended 60% of the tropopause height and were advected at least 10°E longitude and 5°N latitude.

We examined each of the boundary layer trajectories (Fig. 6a) to determine if they agreed with the "reasonably strong" WCB criteria in Eckhardt et al. (2004). The 2 day periods were calculated back from each hourly position along the trajectory path. Results show that 100% of the trajectories met the required northward and eastward displacement criteria during a 2 day period. We then determined whether the trajectories' ascent exceeded 60% of the tropopause height as defined by our WRF simulations. Although the tropopause height varies spatially, its average height in our $30\text{--}60^{\circ}\text{N}$ window (where the ascent occurred) was 10,366 m, agreeing

closely with the values in Eckhardt et al. (2004). Sixty percent of the average tropopause height is 6,219 m. Results show that 71% of the trajectories in Fig. 7a ascended at least this amount during a 48 h period.

Eckhardt et al. (2004) noted that most of the moisture at the start of a WCB is converted to precipitation, thereby producing decreased humidity and an increase in potential temperature. The potential temperatures of their trajectories undergoing WCB processes increased 15-22 K within a 48 h period. We calculated the 48 h change in potential temperature along the leg 5 trajectories in Fig. 6a. Fifty-six percent of them satisfied the criteria of a 15-22 K increase, with 95% of these cases coinciding with ascent greater than 60% of the tropopause height. If we assume that either the horizontal and vertical criteria, OR the horizontal and potential temperature criteria must be met for WCB processes to be verified, our percentage increases from 71 to 74%. Although not all of the leg 5 trajectories satisfy each of the WCB criteria from Eckhardt et al. (2004), many do, and all of the trajectories fulfill the horizontal requirements. These results strongly suggest that most of the trajectories in Fig. 6a did experience “reasonably strong” WCB processes as defined by Eckhardt et al. (2004).

WRF derived constant pressure analyses were examined to determine where the trajectories experienced WCB-related ascent and the pathways that were being followed. Fig. 6a shows the two pathways taken by the trajectories. Transport meteorology associated with the easternmost branch will be examined first. The discussion begins at the source region (where boundary layer air was sampled) and moves forward in time to the aircraft’s location.

Fig. 8 shows average locations of the trajectories comprising the easternmost branch at selected times. The number within each red circle represents the time (in days) prior to the flight encounter. We begin ten days prior to the flight when boundary layer air is sampled (Fig. 8a). The general location of the trajectories is over northeastern Asia, just north of the Koreas. This is an area of major anthropogenic emissions (Fig. 2b). The trajectories are in an area of westerly low level flow at the base of a surface low. This flow persists for the next three days as the trajectories move offshore over the western Pacific to a position south of the Kamchatka Peninsula. Seven days prior to aircraft sampling (Fig. 8b), a new low pressure system strengthens over the Pacific, northeast of the trajectories, keeping the low level westerly flow in place for two additional days (Fig. 8c). Then, a ridge of high pressure forms south of the low,

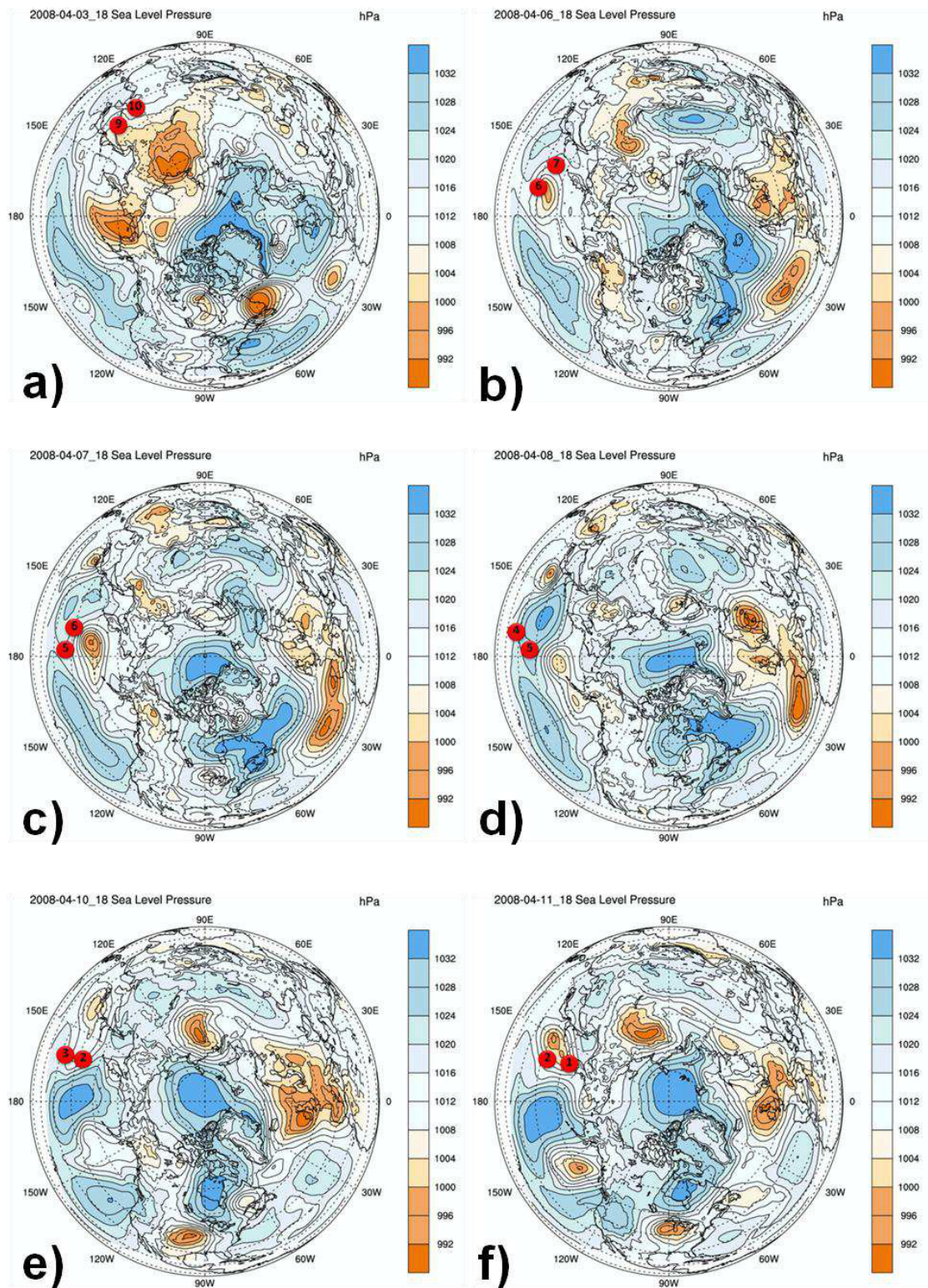


Fig. 8. Red circles denote the average location of trajectories comprising the easternmost branch in Fig. 7a for a) 9-10 days back from the flight, b) 6-7 days back, c) 5-6 days back, d) 4-5 days back, e) 2-3 days back, f) 1-2 days back.

sandwiching the trajectories in between (Fig. 8c). The area of high pressure dominates the low pressure, causing the trajectories to take a southward track along the eastern periphery of the ridge (Fig. 8d). During the next few days the trajectories round the base of the ridge and move to its western periphery two days prior to the flight encounter (Fig. 8e). Meanwhile, a low pressure system develops off the eastern coast of Japan, strengthens, and moves northward, placing the trajectories in the warm sector of the cyclone (Fig. 8f). This is where the trajectories undergo ascent due to the WCB and arrive at the aircraft under the influence of upper level westerly flow. The history of the westernmost branch of trajectories is presented in Fig. 9. Fifteen days prior to aircraft sampling (Fig. 9a), the trajectories are in the boundary layer over southern Asia near Bangladesh and Bhutan. Similar to the eastern branch, this location is an area of major anthropogenic emissions (Fig. 2b). Since the weather pattern at this time is rather benign, the trajectories take a slow, almost negligible, eastward track. At 9 days prior to sampling (not shown), a broad surface low positioned north of the trajectories enhances their eastward progression. They continue eastward over the western Pacific Ocean for the next several days (Fig. 9b). At 4 days prior to the flight (Fig. 9c), they are located just south of Japan along the southeastern quadrant of a developing low pressure system. At 3 days prior to sampling (Fig. 9d) they are east of Japan in the warm sector of the cyclone where they undergo ascent due to the WCB. For the remainder of the time, until reaching the aircraft, they are transported northeastward in the upper troposphere.

In summary, these sections have detailed model-derived transport from Asia, chemical fingerprinting based on in situ aircraft measurements, as well as trajectory and meteorological analyses. The results have shown that chemical tracers specific to Asian and Chinese anthropogenic emissions were sampled during leg 5 of the flight. Trajectory analyses revealed that this air had intersected areas of enhanced anthropogenic emissions across eastern Asia within the boundary layer (Fig. 2b). The emissions then were transported eastward from the Asian continent and underwent WCB related ascent prior to reaching the DC-8 at flight level on 12 April 2008.

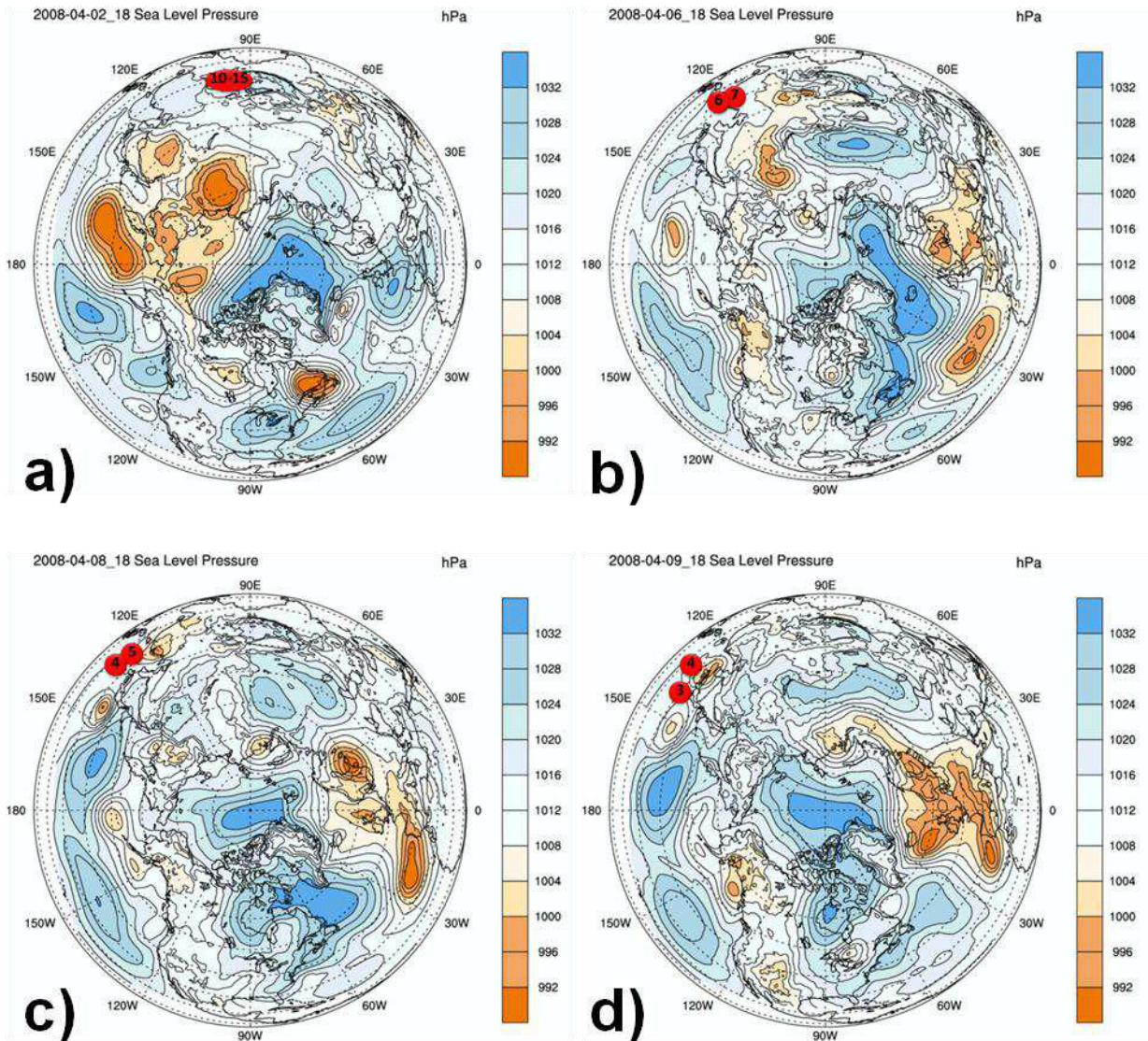


Fig. 9. Red circles denote the average location of trajectories comprising the westernmost branch in Fig. 7a for a) 10-15 days back from the flight, b) 6-7 days back, c) 4-5 days back, d) 3-4 days back.

3.4 North American Transport during ARCTAS-A

We next examine the transport of North American anthropogenic emissions to the Arctic. One hundred and seventy-eight trajectories were released over North American anthropogenic sources (Fig. 2c, d) each day during ARCTAS-A, producing a total of 5518 releases during the 31 day period. Similar to the Asian domain, the distribution of Arctic arrivals favors the northern half of the region (Fig. 10a). Origins at latitudes greater than 40°N produce 47% of the

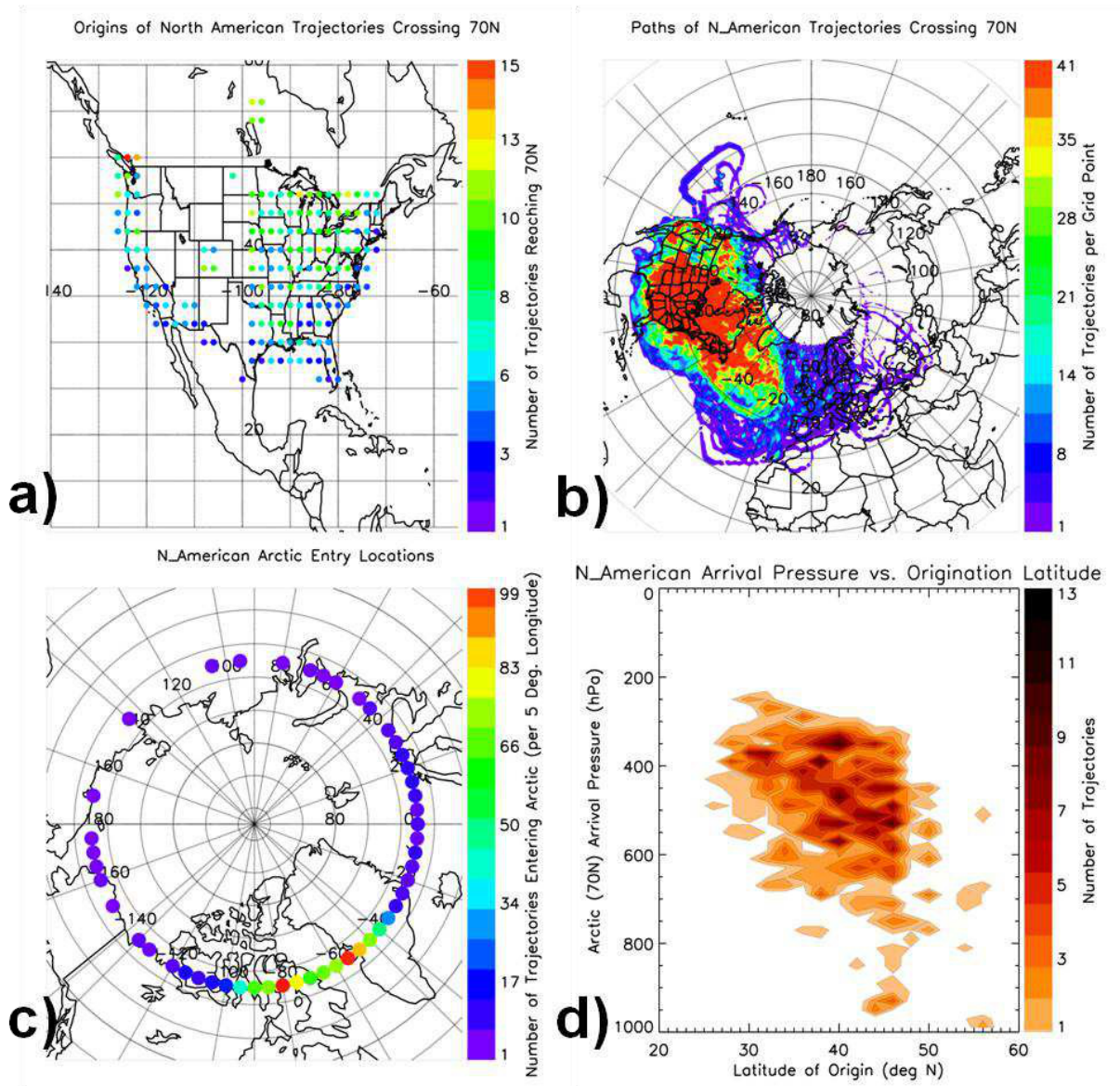


Fig. 10. As in Fig. 4, but for North American trajectories.

Arctic bound trajectories, while 50% of the trajectories originate between 30-40°N. Only a small percentage (3%) of trajectories originating at latitudes less than 30°N reach the Arctic. A close examination of the trajectories crossing 70°N (Fig. 10b), reveals two pathways, one is distinct, and the other is less defined. The most distinct pathway transports air north from their release points. This path continues across northeastern Canada and enters the Arctic over Baffin Bay. The less defined pathway takes trajectories eastward across the North Atlantic Ocean and over Europe. From there they disperse and enter the Arctic in a disorganized pattern.

Entry regions to the Arctic (70°N) are shown in Fig. 10c. The most prominent entrance region is between Nunavut, Canada and Greenland, a common pathway seen in Fig. 10b. Of the trajectories that enter the Arctic from North America, 85% arrive between 40-100°W. A much smaller percentage (14%) enters the Arctic across northern Europe between 40°W and 40°E. This region also is depicted in Fig. 10b. The remaining 1% enters the Arctic sporadically along the 70°N latitude ring.

The distribution of altitudes at which trajectories arrive in the Arctic (Fig. 10d) is similar to that for the Asian domain (Fig. 4d). Most trajectories arriving from North America enter the Arctic in the middle (42%) and upper troposphere (53%); only 5% arrive in the lower troposphere. These pathways are consistent with previous studies (i.e., Stohl, 2006; Law and Stohl, 2007; Klonecki et al., 2003).

3.5 North American Case Study

DC-8 flight 5 on 5 April 2008 is an example of transport from North America to the Arctic. Leg 8, between 16:27-17:13 UTC, is shown in Fig. 3a as the red segment between Baffin Island, Canada and Disko Bay, Greenland.

3.5.1 Chemical Fingerprinting

Volatile organic compounds, including nonmethane hydrocarbons (NMHCs), generally reach maximum concentration over the United States during the winter months when OH production and photochemistry are at a seasonal minimum (Russo et al., 2010). Concentrations decline during spring, reaching a minimum during the summer months when photochemistry is most active. Some of these VOCs undergo chemical reactions in the presence of nitrogen oxides to produce ozone, a component of photochemical smog (Carter, 1994; Russo et al., 2010). It is important to note that NMHCs from urban locations in the United States primarily are anthropogenic (Lee et al., 2006).

An examination of the incomplete combustion (IC) tracer C_6H_6 (Fig. 11c), as well as two purely anthropogenic tracers (HCFC-22 and C_2Cl_4 , Figs. 11d, e), whose origins have been discussed in the previous case study, exhibit enhancements along leg 8. Since our IC tracer can have either biomass burning or anthropogenic origins, we correlated it with the known anthropogenic species C_2Cl_4 to determine its source. The two are well correlated ($r^2 = 0.72$),

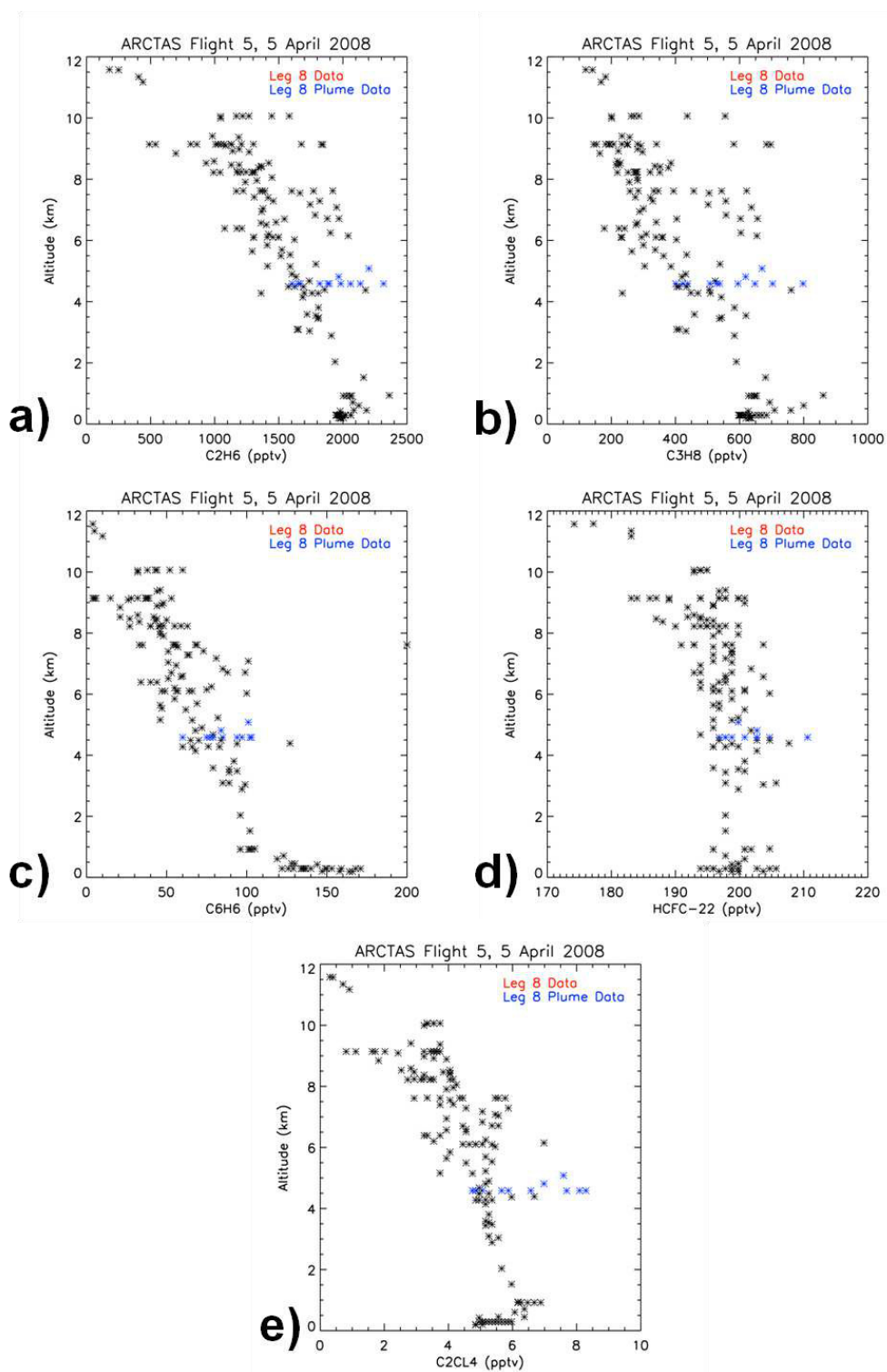


Fig. 11. Vertical distribution plots for data from flight 5 on 5 April 2008 for a) C_2H_6 , b) C_3H_8 , c) C_6H_6 , d) HCFC-22, and e) C_2Cl_4 . Blue points are from leg 8, representing the sampled plume. In this case the plume is represented by all of the data points along leg 8. Black points represent the remaining legs of flight 5.

thus, we can assume C_6H_6 has anthropogenic sources. In addition, C_2H_6 and C_3H_8 (also enhanced along leg 8, Figs. 11a, b, respectively), two natural gas tracers that also are emitted from biomass burning, show good correlation ($r^2 = 0.86$ and $r^2 = 0.90$, respectively) with the anthropogenic tracer C_2Cl_4 . Therefore, the data suggest that an urban/industrial influence is much more likely than a biomass burning influence.

Fig. 11 presents the species listed above with respect to altitude during the 5 April 2008 flight. Similar to the previous figure of this type (Fig. 5), data for flight legs other than leg 8 are in black. However, since all data points in the North American leg represent the sampled plume, the entire suite of data for leg 8 is colored in blue. These data were determined to be from the same plume since they all experienced enhancements over their respective background values, and they were sampled in the same altitude range (4500-5000 m).

Similar to Table 2, Table 3 presents mean background mixing ratios during ARCTAS-A (for the species discussed above) for comparison with mean mixing ratios from the plume sampled along leg 8. The species listed in Table 3 exhibit higher mixing ratios in the leg 8 North American plume than in the background air. Mean values of C_3H_8 , C_6H_6 , C_2Cl_4 , C_2H_6 , and HCFC-22 in the North American plume are enhanced by 83, 76, 51, 37 and 3%, respectively, over their mean background values (Table 3).

In summary, two purely anthropogenic species (C_2Cl_4 and HCFC-22) were enhanced over the background in the North American plume. Tetrachloroethene correlated well with benzene, a non-specific tracer of incomplete combustion, as well as two natural gas tracers (C_3H_8 and C_2H_6), strongly suggesting anthropogenic rather than biomass sources. These data suggest that the DC-8 sampled anthropogenic emissions along leg 8 of the ARCTAS flight on 5 April 2008. The North American source is examined further in the next section.

Table 3. As in Table 2, but for the North American plume.

Compound	Formula	Lifetime	LOD (pptv)	Precision (%)	Accuracy (%)	Bkgd. Avg. (pptv)	Bkgd. St. Dev. (pptv)	North American Plume Avg. (pptv)	North American St. Dev. (pptv)	Enhancement over average background (%)	North American Plume Max (pptv)
Ethane	C ₂ H ₆	47 d	3	1	5	1408	166	1932	225	37	2317
Propane	C ₃ H ₈	11 d	3	2	5	312	59	573	122	83	798
Benzene	C ₆ H ₆	9 d	3	3	5	49	12	86	13	76	103
HCFC-22	HCFC-22	12 yr	2	5	5	195	2	201	4	3	210
Tetrachloroethene	C ₂ Cl ₄	2-3 mo	0.01	5	10	4.20	0.60	6.35	1.36	51	8.29

3.5.2 Transport and Meteorology

Forty-seven 15 day backward trajectories were released each minute along flight leg 8 within the 600-500 hPa layer. As before, each trajectory was examined to determine whether it entered the boundary layer along its path; 39 trajectories were found to have done so (Fig. 12a). Most of these trajectories follow a complex looping path as described below. Although, a few travel westward across the United States and encounter the clean boundary layer of the northern Pacific Ocean, the majority of boundary layer occurrences are located along the east coast of North America (Fig. 12b). After release from the aircraft, these trajectories travel south within the upper troposphere and shift more southeasterly by day 2. They then change direction and begin to descend and transit westward across the extreme northwestern Atlantic. They next turn southward and continue to descend to a position off the northeastern coast of the U.S. The trajectories experience another change in direction toward the west to the middle Atlantic coastline. Upon reaching the coastline, they reverse course and track back over the Atlantic. Finally, they turn back to the north and travel across Prince Edward Island before returning to a location near the region of their aircraft release by day 15.

It is important to know where the leg 8 trajectories encounter the North American boundary layer. Fig. 12b shows those trajectory segments in Fig. 12a that are within the boundary layer. A majority of the boundary layer segments are located along the eastern U.S. coastline and just offshore over the western Atlantic. Some segments also are located in the central U.S. and eastern Canada. Most of these locations correspond to areas of enhanced anthropogenic emissions (Fig. 2d).

Fig. 12c shows deep ascent beginning ~ 4 days prior to sampling. The methods used previously to define “reasonably strong” WCB transport (Eckhardt et al., 2004) again were employed. All of the trajectories examined along leg 8 satisfy the horizontal WCB requirements. The tropopause height was calculated between 40°N and 60°N, yielding an average height of 9644 m, with 60% of this value being 5787 m. Although 44% of the trajectories meet the potential temperature criterion, none satisfy the ascent criterion. However, if we reduce the vertical criterion to 40% of the tropopause height (3858 m), 72% of the trajectories satisfy the requirement. Furthermore, 94% of those satisfying the potential temperature criteria coincide with those that satisfy the revised ascent criterion. Considering horizontal motion, the change in potential temperature, and the reduced ascent criterion, 74% of the examined leg 8 trajectories

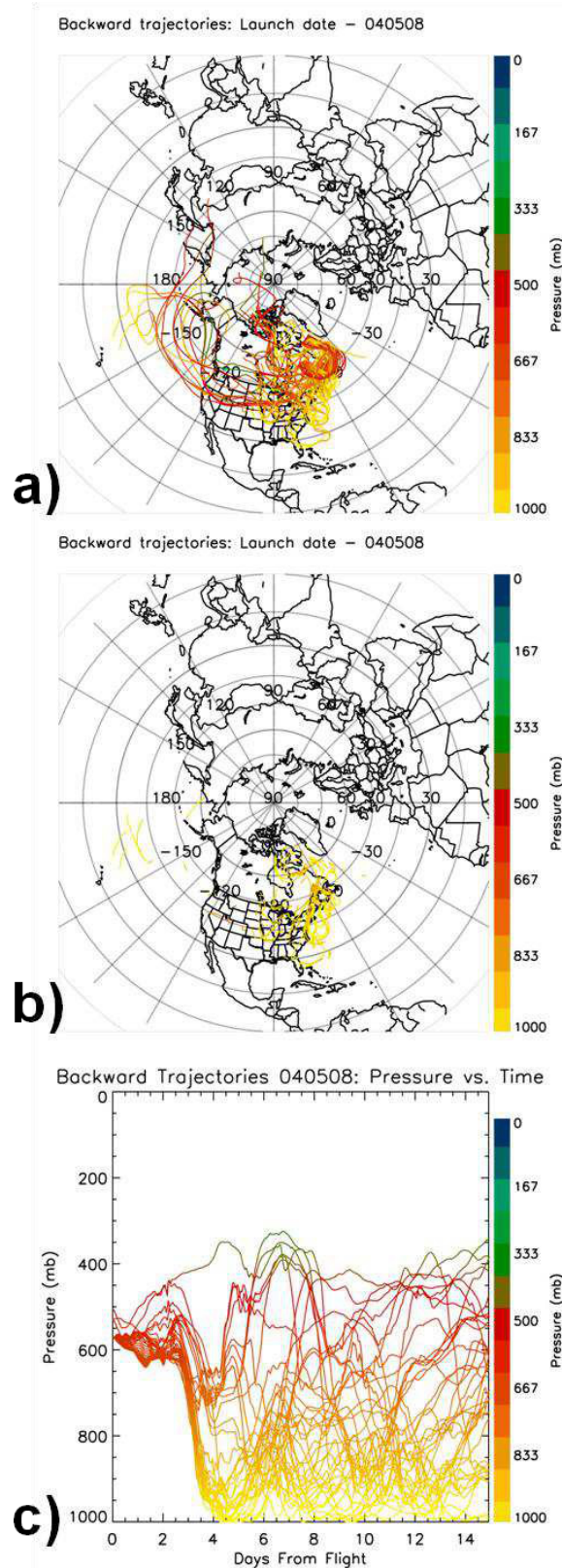


Fig. 12. As in Fig. 6, but for leg 8 on 5 April 2008.

satisfy the revised WCB requirement. It is important to note the strong seasonal variability in WCB frequency and associated vertical mass flux, with maxima during winter and minima in summer (Stohl, 2001; Eckhardt et al., 2004). Since ARCTAS-A occurred during a transitional season, the 60% ascent requirement may be too strict for spring, causing valid WCBs to be neglected. This information and the synoptic patterns described below indicate that the leg 8 trajectories did experience ascent due to a WCB.

We next relate the looping paths of the leg 8 trajectories with weather patterns during the 15 day transit period (Fig. 13). Fifteen days prior to the DC-8 sampling anthropogenic emissions (not shown), the average location of the trajectories is over Baffin Bay, close to the sampling location. They move along the western periphery of a broad surface low southwestward to Hudson Bay 13 days prior to sampling. The surface low then translates westward, with the trajectories on its southern edge where they move eastward over the eastern Labrador Sea. The low begins to weaken, and the trajectories move into stagnant flow over the northern Labrador Sea, just south of Baffin Island. A surface low strengthens just east of Greenland, providing enough southerly flow to advect the trajectories to near Prince Edward Island by 8 days prior to the flight. At this point, a broad high pressure ridge strengthens across the eastern United States, placing the trajectories in a region of northerly flow on its eastern edge. The ridge strengthens further and moves eastward over the western Atlantic as the trajectories continue moving south along its eastern periphery (Fig. 13a and b). The trajectories round the base of the ridge 6 days prior to sampling as the ridge continues to move eastward. This transports them westward to a point along the northeastern U.S. coastline at five days prior to the flight. It is between 4 and 5 days back from the flight that the most trajectories encounter the boundary layer along the North American coastline where anthropogenic emissions are at their greatest (Fig. 2d). Then, a surface low strengthens over the Great Lakes, placing the trajectories between the ridge and the cyclone, in a region of southwesterly flow. They move northeastward toward Prince Edward Island (Fig. 13c). The low then strengthens and transports the trajectories into its warm sector 3 days prior to the flight (Fig. 13d). It is here that the trajectories undergo WCB related ascent that lofts them into the upper troposphere. Finally, they round the base of an upper trough before travelling northwestward to the DC-8.

To summarize, chemical fingerprinting and meteorological analyses indicate that the DC-8 sampled North American anthropogenic emissions during leg 8 of the 5 April 2008 flight.

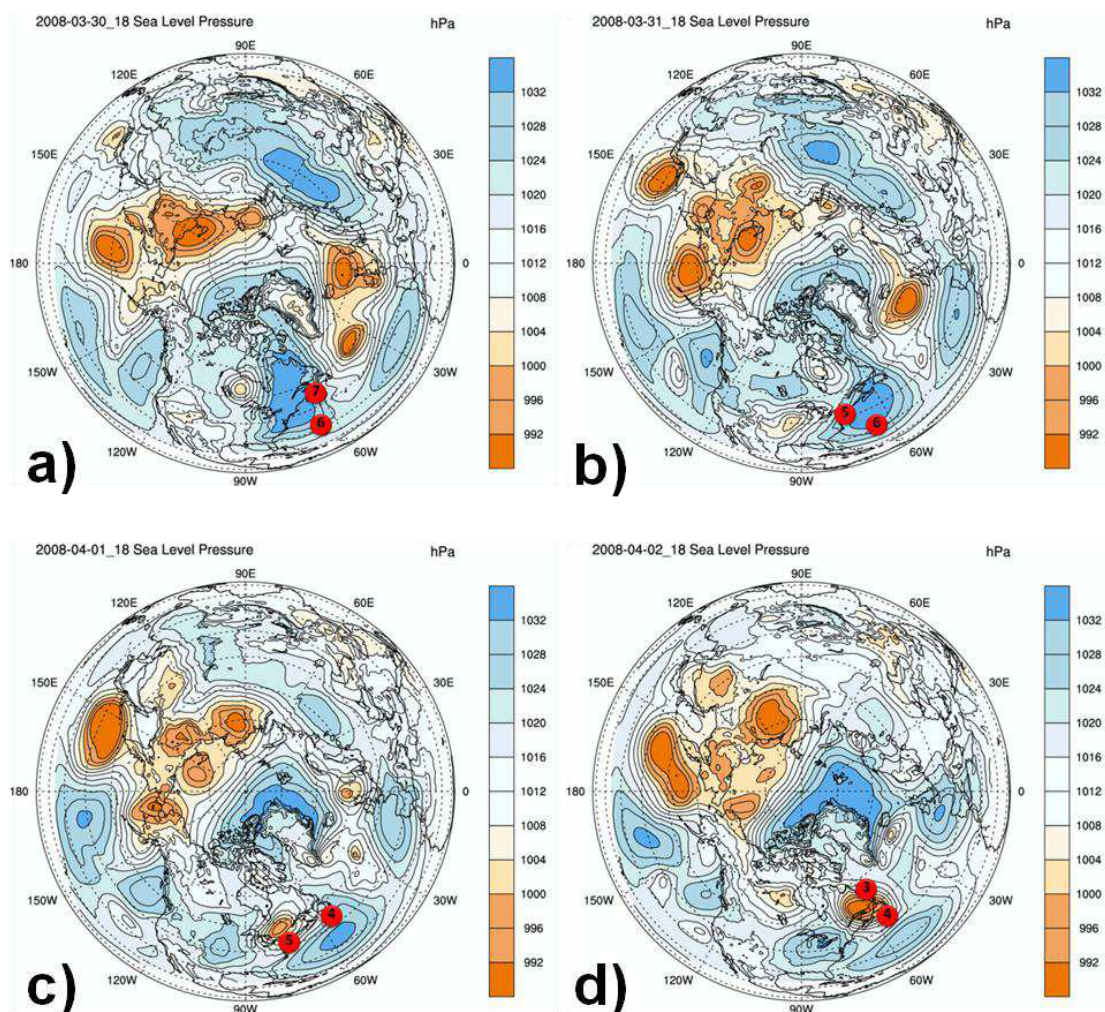


Fig. 13. Average positions of the group of trajectories released from leg 8 of the DC-8 flight on 5 April 2008. Red circles denote locations at a) 6-7 days back from the flight, b) 5-6 days back, c) 4-5 days back, and d) 3-4 days back.

Vertical distribution plots and comparisons with background mixing ratios revealed enhancements during this leg, including tracers having purely anthropogenic sources. Trajectory analysis showed that boundary layer air was encountered along the northeastern U.S. coast where anthropogenic emissions are a maximum (Fig. 2d). Finally, the trajectories underwent WCB related ascent to the middle troposphere where the emissions were sampled by the DC-8

3.6 European Transport during ARCTAS-A

Two hundred and twenty-four 15 day forward trajectories were launched on each of the 31 ARCTAS-A days from our European area of anthropogenic emissions (Fig. 2e, f), resulting in a total of 6,944 releases. Only a few release points in the far southeastern domain do not produce Arctic bound trajectories (Fig. 14a). Of the total trajectories released, 1,936 (28 %) reach the Arctic within 15 days. Trajectories released at latitudes greater than 50°N account for 32% of the trajectories entering the Arctic (70° N). Fifty-four percent of the trajectories released between 40°N and 50°N reach the Arctic, while latitudes less than 40°N account for the remaining 14%. Trajectories reaching the Arctic follow two distinct pathways (Fig. 14b). The first transports emissions northward across northern Europe. These trajectories cross 70°N and then turn eastward and continue within the Arctic Circle. This path is most common for trajectories that remain in the lower troposphere. The second common pathway begins with the trajectories moving eastward from the domain. They cross Turkey and continue eastward across the northern Middle East and then to the Arctic. Although this pathway is most common for trajectories in the middle and upper troposphere, some trajectories in the middle and upper levels follow the first pathway.

Locations over northern Europe and northeastern Russia are the dominant entry region to the Arctic for trajectories originating from European domain (Fig. 14c). This 70° longitude region between 20-90°E accounts for 62% of the trajectories entering the Arctic. Two interesting features in Fig. 14c are the increased number of trajectories entering the Arctic in the same regions observed for Asian and North American trajectories (Figs. 4c and 10c, respectively). The longitude sector between 180°W and 140°W was a frequent entry region for Asian emissions (61.5%), and it accounts for 6% of the trajectories entering the Arctic from Europe. Likewise, the region between 100°W and 40°W was a common entry region for North American trajectories (85%), and it accounts for 7% of the trajectories released from the European domain.

The altitudes at which European trajectories enter the Arctic (Fig. 14d) differ from the previous two domains (Figs. 4d and 10d). European releases arrive in the lower, middle, and upper troposphere, whereas trajectories from the previous domains were primarily in the middle and upper troposphere. Although the middle troposphere accounts for 56% of the European releases reaching the Arctic, the lower levels account for 17%. This percentage arriving in the

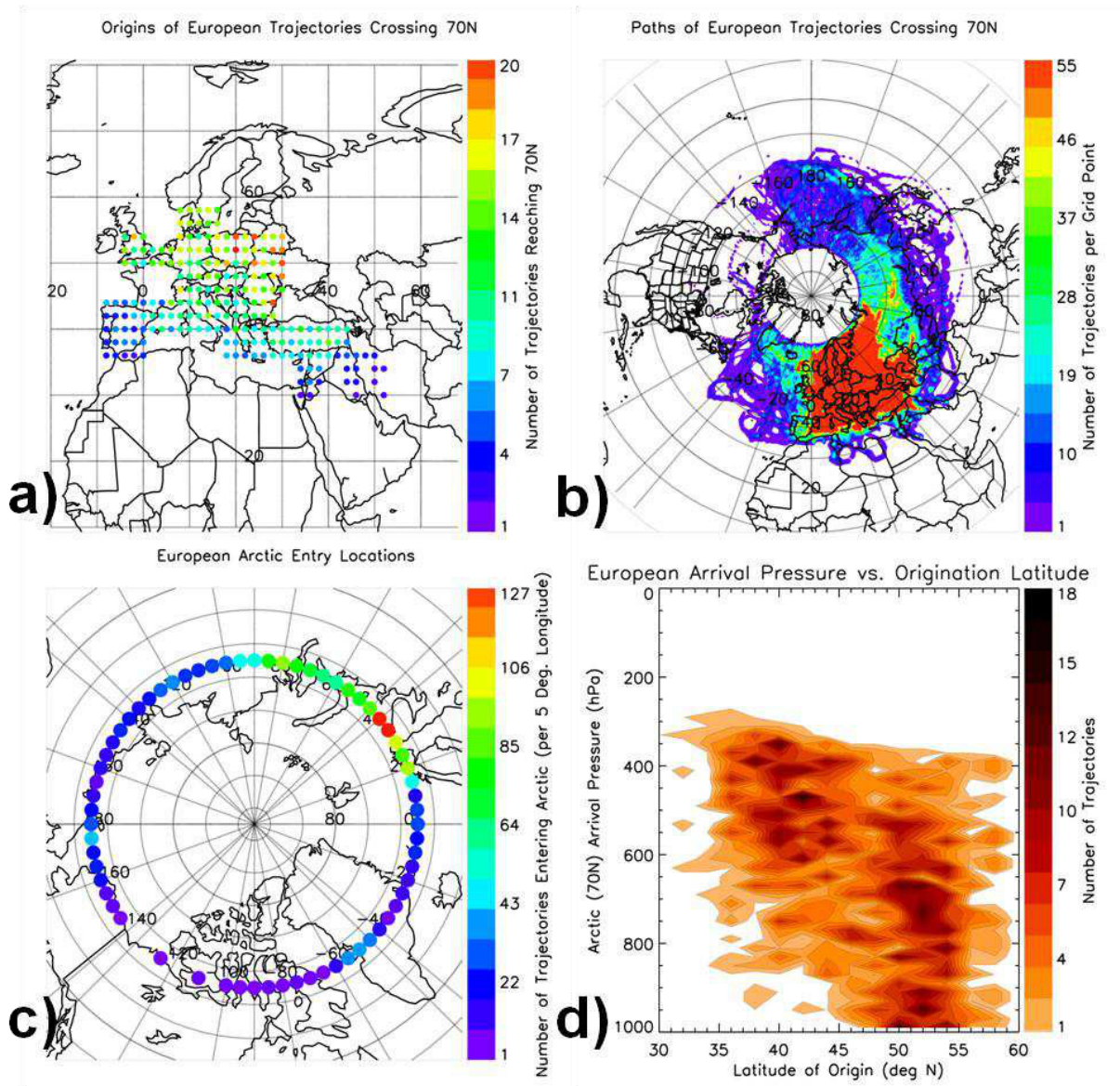


Fig. 14. As in Fig. 4, but for trajectories released from areas of European anthropogenic emissions.

lower troposphere is considerably greater than the previous two regions (3% from Asia and 5% from North America). This finding of European arrivals in the lower troposphere is consistent with Klonecki et al. (2003), Stohl (2006), and Law and Stohl (2007). The remaining 27% of Arctic bound trajectories from Europe arrive in the upper levels.

3.7 European Case Study

Data from DC-8 flight 8 on 12 April 2008 comprise our case study of European emissions. This is the same flight on which Asian emissions were sampled, emphasizing the finding that many ARCTAS-A flights sampled air with multiple origins. The case focuses on the period 18:26-18:55 UTC which is denoted leg 8 (leg 5 was studied for the Asian case). Leg 8 is located across the Bering Strait and over St. Lawrence Island, AK (Fig. 3b).

3.7.1 Chemical Fingerprinting

We are not aware of previous research that provides a chemical fingerprint that is specific to European anthropogenic emissions. Thus, chemical considerations will not definitively link the sampled plume to a European source. Rather, the firm linkage with Europe will be based on trajectory and meteorological analyses.

The species examined for this case study are C_2Cl_4 , C_2H_2 , C_6H_6 , C_2H_6 , C_3H_8 , and methane (CH_4) (Fig. 15). Similar to the other cases, the blue points (in Fig. 15) represent the sampled plume along leg 8. This plume consists of 3 data points at almost the same altitude between 3704-3708 m.

Each of the tracers being examined has been used and discussed in previous sections with the exception of CH_4 . Methane is introduced because when CH_4 , C_3H_8 , and C_2H_6 are well correlated, natural gas emission can be inferred (Section 2.3). However, since CH_4 , C_3H_8 , and C_2H_6 emissions can be from both biomass and anthropogenic sources, further examination is needed. First, the correlation for each of the natural gas tracers with the others was computed. The best correlations are between C_2H_6 and C_3H_8 ($r^2 = 0.95$), followed by CH_4 and C_3H_8 ($r^2 = 0.76$), and CH_4 and C_2H_6 ($r^2 = 0.56$). In addition to some strong mutual correlations, this trio of gases also exhibits excellent correlation with the urban/industrial tracer C_2Cl_4 ($r^2 = 0.91$, 0.83 and 0.96 for CH_4 , C_2H_6 , and C_3H_8 , respectively). This strongly suggests that CH_4 , C_2H_6 and C_3H_8 were co-emitted from urban/industrial natural gas usage, and not from biomass burning. Finally, the two IC tracers (C_2H_2 and C_6H_6) also show excellent correlation with C_2Cl_4 ($r^2 = 0.99$ and 0.73 , respectively), again consistent with an urban/industrial combustion source and not biomass burning.

Following the methods in Sections 3.3.1 and 3.5.1, Table 4 presents mean background mixing ratios during ARCTAS-A for the tracers used in this case, as well as mean values for the

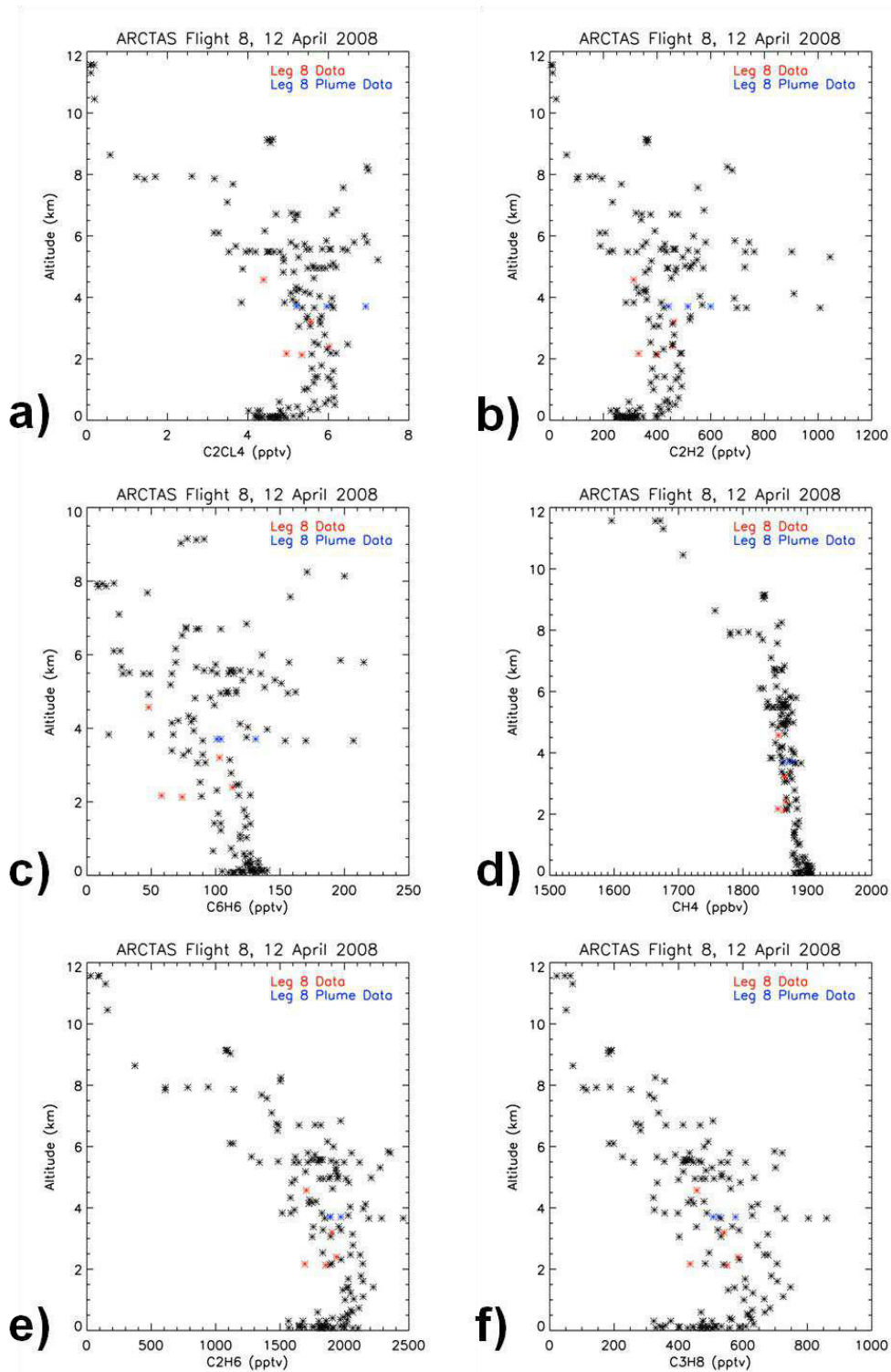


Fig. 15. Vertical distribution plots for data from flight 8 on 12 April 2008 for a) C_2Cl_4 , b) C_2H_2 , c) C_6H_6 , d) CH_4 , e) C_2H_6 , and f) C_3H_8 . Red points are data from leg 8. Blue points also are from leg 8 but represent the sampled plume. Black points represent the remaining legs of flight 8.

Table 4. As in Table 2, but for the European plume.

Compound	Formula	Lifetime	LOD	Precision	Accuracy	Bkgd. Avg. (pptv)	Bkgd. St. Dev. (pptv)	European Plume Avg. (pptv)	European St. Dev. (pptv)	Enhancement over average background (%)	European Plume Max (pptv)
Tetrachloroethene	C ₂ Cl ₄	2-3 mo	0.01	5	10	4.20	0.60	6.03	0.86	44	6.93
Ethyne	C ₂ H ₂	12-17 d	3.00	3	5	264	42	519	79	97	600
Benzene	C ₆ H ₆	9 d	3.00	3	5	49	12	112	17	129	131
Methane (ppbv)	CH ₄	9 yr	n/a	1	1	1840*	8*	1871*	8*	2	1877*
Ethane	C ₂ H ₆	47 d	3.00	1	5	1408	166	1917	47	36	1972
Propane	C ₃ H ₈	11 d	3.00	2	5	312	59	537	36	72	577

* Units for methane mixing ratios are ppbv.

sampled plume along leg 8. Similar to the previous two cases, the species in Table 4 have higher mixing ratios in the leg 8 European plume than in background air measured during ARCTAS-A. Mean values of C_6H_6 , C_2H_2 , C_3H_8 , C_2Cl_4 , C_2H_6 , and CH_4 in the European plume are enhanced by 129, 97, 72, 44, 36 and 2%, respectively, over their mean background values (Table 4).

In summary, enhancements in the purely anthropogenic tracer C_2Cl_4 indicate that our plume is of anthropogenic origins. Good correlations between CH_4 , C_2H_6 , C_3H_8 , C_2Cl_4 , C_6H_6 and C_2H_2 also strongly suggest anthropogenic emissions that include both natural gas and combustion sources. Thus, it is clear that along leg 8 of flight 8 on 12 April 2008, the DC-8 sampled anthropogenic emissions. The source of these emissions will be examined in the next section.

3.7.2 Transport and Meteorology

Of all the DC-8 flights during April, flight 8 provides the most favorable trajectories for sampling boundary layer air over Europe, while avoiding large areas of biomass burning. Thirty backward trajectories were released each minute along leg 8 within the 850-500 hPa layer, with 13 of them traveling in the boundary layer at some time during their 15 day transit (Fig. 16a). The remaining 17 trajectories released along leg 8 follow pathways that are similar to the boundary layer trajectories, but always remain above the boundary layer. The paths of the boundary layer trajectories (Fig. 16a) are simple compared to the previous cases. After being released along the flight track, they travel westward between 50-70°N through the middle and upper troposphere. As they pass over the Kamchatka Peninsula, two pathways become apparent. The smallest group, consisting of only 3 trajectories, moves westward along 60°N and eventually descends to the lower troposphere in central Russia. The remaining group crosses 60°N several times and continues further west than the previous group, travelling along 70°N. They then make an abrupt turn and descend over Finland. Once in the lower troposphere, the group splits into two branches. One travels west over Germany while the other travels east over northern Ukraine.

Knowing where the trajectories were in the boundary layer is especially important in this case because of a large area of fires across western Russia. Figure 17 shows a close up view of the trajectories from Fig. 16a, as well as a composite of all fire locations between 26 March and 6 April 2008 (the period when the trajectories were over Europe and Russia). Fire locations are

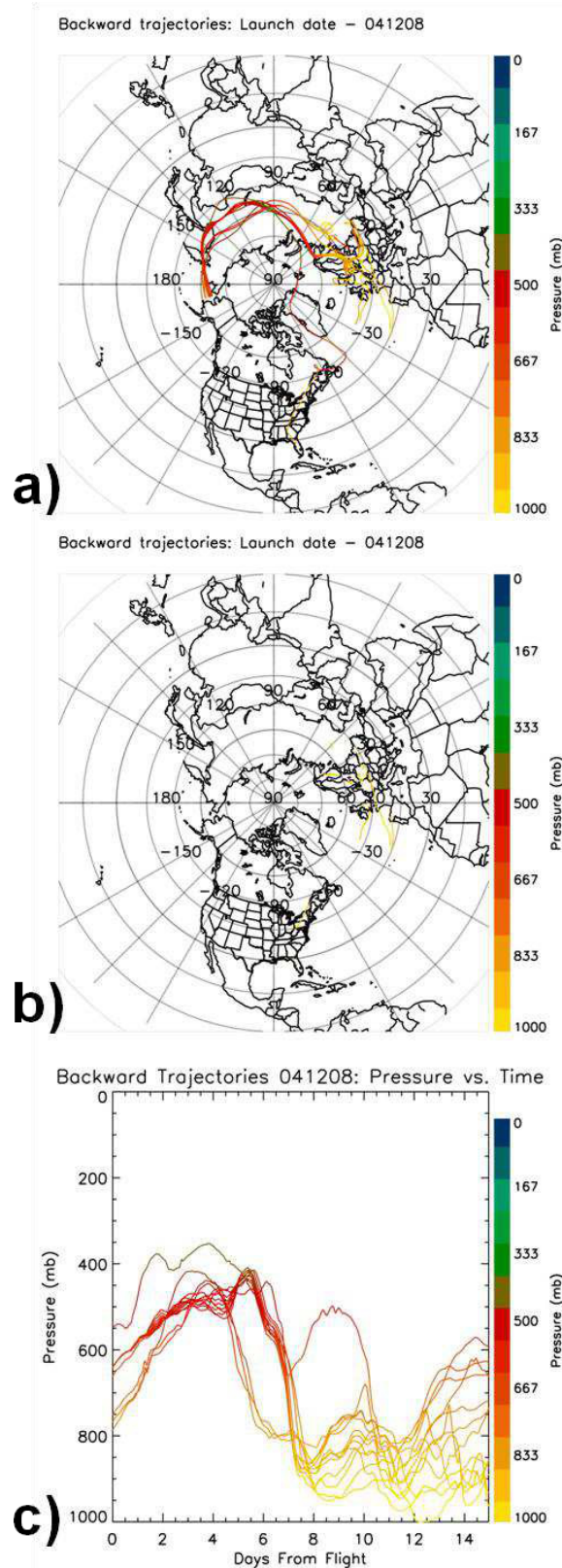


Fig. 16. As in Fig. 6, but for leg 8 on 12 April 2008.

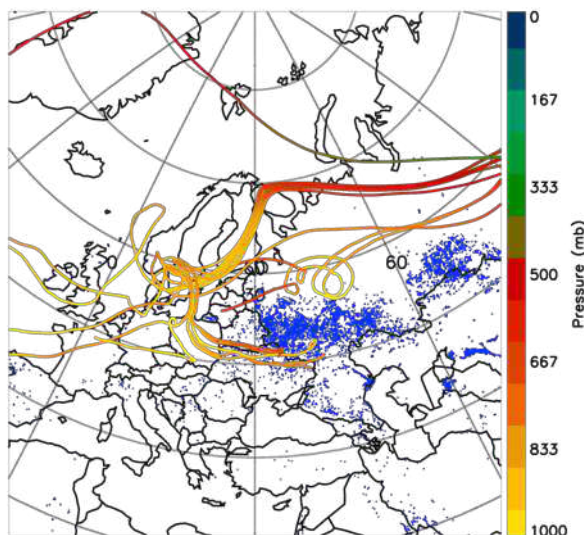


Fig. 17. Trajectories as in Fig. 18a plotted with FLAMBE data (blue dots) for the period 26 March - 6 April 2008.

from the Naval Research Laboratory (NRL) Fire Locating and Modeling of Biomass Burning Emissions (FLAMBE) dataset (Reid et al., 2009). The fires primarily are located between 50-60°N, with the westernmost boundary across eastern Belarus and northeastern Ukraine. Fig. 16b shows the boundary layer segments of the trajectories in Fig. 16a. A few trajectories have brief encounters with the boundary layer over western Russia, near the large region of fires. These brief encounters were not evident in the chemistry described in earlier sections. Most trajectories encounter the boundary layer across Europe, where fires are virtually absent.

Fig. 16c presents the trajectories from Fig. 16a in a pressure versus time reference. Synoptic scale ascent is indicated between ~ 8-6 days prior to sampling. Potential WCB influences again were investigated using the criteria in Eckhardt et al. (2004). Ninety-two percent of the 13 trajectories examined satisfy the horizontal WCB criteria. The average tropopause height of 9584 m was calculated in the latitude belt 60-70°N, with 60% of this value being 5751 m. Only 1 of the 13 trajectories satisfies the 48 h ascent requirement. Similar to the previous section, if the ascent criterion is decreased to 40% of the tropopause height (3834 m) during a 48 h period, 62% of the 13 trajectories meet the revised requirement. It is important to remember that Fig. 16a shows two separate groups of trajectories. The smaller group is not suspected to have undergone WCB processes. If we remove these 3 “stray” trajectories, 80% of

the remainder satisfies the revised WCB requirements. Therefore, we believe the trajectories' large scale ascent again is due to a WCB.

Meteorological analysis supports our hypothesis of WCB related ascent, and it explains the pathways taken by the trajectories in Fig. 16a. Fig. 18 shows the average locations of the 15 day backward trajectories from leg 8. They begin near 30°W over the northern Atlantic Ocean in a region of westerly flow along the base of a deep surface cyclone (not shown). The trajectories continue in this westerly flow for several days as the low pressure system weakens (Fig. 18a-d). When the trajectories are near Poland, 11 days prior to sampling, the flow becomes stagnant. Over the next two days, the trajectories drift eastward as a surface low develops over the Atlantic and moves onshore near Norway. At 9 days prior to DC-8 sampling (Fig. 18e), they are on the eastern edge of the newly developed cyclone. As the low continues its eastward progression, the trajectories pass into the cyclone's warm sector where they ascend due to the WCB (Fig. 18f). Once the trajectories are lofted into the upper levels, they are transported by the westerlies and are sampled by the DC-8 7 days later.

In summary, these results strongly suggest that the DC-8 sampled anthropogenic emissions along leg 8 of the 12 April 2008 flight. Vertical distributions showed enhancements in the purely anthropogenic tracer C_2Cl_4 , as well as in natural gas tracers CH_4 , C_2H_6 , and C_3H_8 , determined to be of anthropogenic origins. The IC tracers C_2H_2 and C_6H_6 were shown to be of anthropogenic origin as well. Trajectory analysis showed that boundary layer influences occurred across European locations associated with enhanced anthropogenic emissions (Fig. 2f). The leg 8 trajectories were lofted into the upper troposphere by a WCB, where they were subsequently sampled by the DC-8. Although the pathway taken by these trajectories was common during ARCTAS-A (Sect. 3.6), they did not enter the Arctic in the most common region (northern Europe/northeastern Russia, Fig. 14c). Instead, the trajectories entered the Arctic through one of the secondary "hot spots" (Fig. 14c). This secondary location, north of the Bering Strait is shared by emissions from Asia (Fig. 4c).

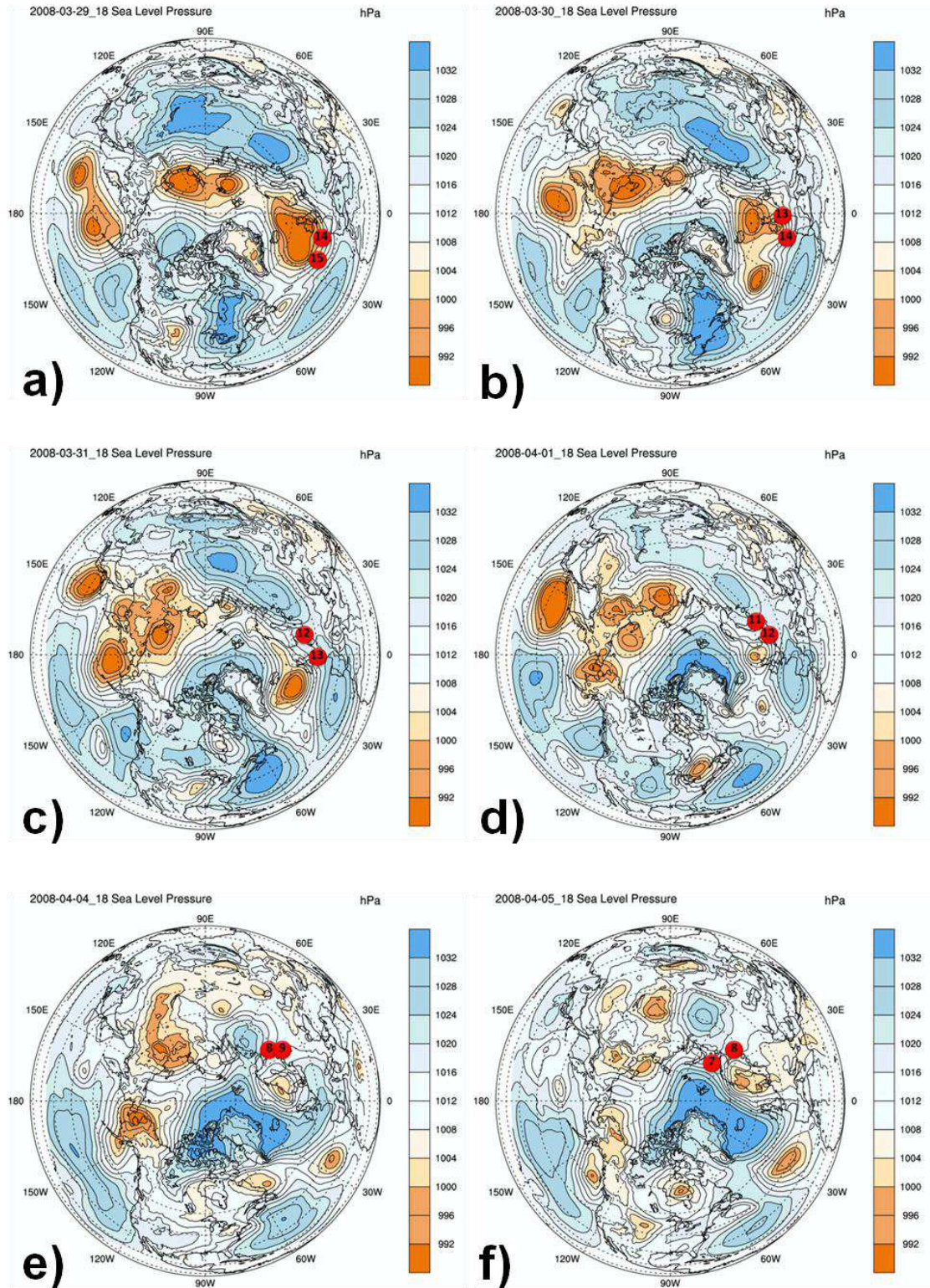


Fig. 18. Red circles denote the average location of trajectories comprising the largest group of trajectories in Fig. 18a for a) 14-15 days back from the flight, b) 13-14 days back, c) 12-13 days back, d) 11-12 days back, e) 8-9 days back, and f) 7-8 days back.

CHAPTER 4

SUMMARY AND CONCLUSIONS

This study has examined the transport of anthropogenic emissions to the Arctic during NASA's Arctic Research of the Composition of the Troposphere from Aircraft and Satellites (ARCTAS) field mission conducted during 2008 (Jacob et al., 2010). Our focus was the spring phase of ARCTAS (ARCTAS-A) that occurred during April. Although biomass burning emissions dominated pollution transport to the Arctic during the study period (Warneke et al., 2009; Jacob et al., 2010), our goal was to document the Arctic transport and meteorology associated with anthropogenic emissions. Three source regions were studied—Asia, North America, and Europe. Meteorological data were obtained from high resolution simulations using the Weather Research and Forecasting (WRF) model. We computed statistics describing common pathways, origins, and entry regions for emissions entering the Arctic (defined as 70° N) during the complete ARCTAS-A period. We also presented a detailed case study for each source region using DC-8 aircraft-derived in situ data and backward trajectories.

Leg 5 from DC-8 flight 8 on 12 April 2008 was found to have sampled anthropogenic emissions originating from eastern Asia. Results showed enhancements of several key tracers (OCS, CH₃Cl, 1,2 DCE, and H-1211) that Barletta et al. (2009) have linked to eastern Asian anthropogenic emissions. Values of the purely anthropogenic species HCFC-22 and C₂Cl₄ also were enhanced along this leg. Carbonyl sulphide and CH₃Cl, two tracers that could have either biomass or anthropogenic origins, were highly correlated with the anthropogenic tracer C₂Cl₄, which led to the conclusion that both tracers had anthropogenic origins.

Fifteen day backward trajectories released from leg 5 were traced back to origins across eastern Asia. They originated along the eastern Asian coast and passed through the boundary layer in regions of anthropogenic emissions. The pathway, origin, and Arctic entry locations of this case study were consistent with those of the entire ARCTAS-A period. Meteorological analyses highlighted the importance of synoptic scale cyclones and anticyclones in transporting the emissions. The results also illustrated the importance of a warm conveyor belt (WCB) in transporting the emissions to higher altitudes where they were sampled by the DC-8. Based on

its chemical signature and backward trajectories, leg 5 was concluded to exhibit an anthropogenic influence.

The transport of Asian anthropogenic emissions also was investigated each day during ARCTAS-A, producing a “climatology” of the period. Asian emissions during ARCTAS-A most commonly were transported eastward across the northern Pacific Ocean and then lofted into the upper levels. The coast of eastern Asia is a common location for the development of strong WCBs (Eckhardt et al., 2004), and we hypothesize that Asian transport to the Arctic often is facilitated by them. These emissions usually passed northward through the Bering Sea where they crossed 70°N latitude and entered the Arctic. Results showed that emissions from Asia most commonly entered the Arctic in the middle and upper levels during ARCTAS-A. Emissions that originated from higher latitudes across eastern Asia tended to arrive in the middle troposphere, while emissions originating at lower latitudes more commonly arrived in the upper troposphere.

Results showed that anthropogenic emissions from North America were sampled along leg 8 of DC-8 flight 5 on 5 April 2008. This period served as our case study. Enhanced mixing ratios of several species, including two having strictly anthropogenic origins (C_2Cl_4 and HCFC-22), were found along the leg. The incomplete combustion tracer C_6H_6 exhibited a good correlation with the purely anthropogenic tracer C_2Cl_4 and was determined to have anthropogenic origins. Similarly, two natural gas tracers (C_2H_6 and C_3H_8) also correlated well with C_2Cl_4 indicating their origins were from anthropogenic sources.

Backward trajectories released along leg 8 spent considerable time over North America. They were within the boundary layer over regions of known anthropogenic emissions (i.e., the eastern U.S. coastline from Connecticut south to Virginia and the Midwest states). Since WCBs frequently originate east of North America (Eckhardt et al., 2004), it was not surprising that a WCB was responsible for the vertical transport of these emissions to their sampling locations at the DC-8.

The transport pathway of the North American case was consistent with transport statistics for the entire ARCTAS-A period. Emissions from North America generally traveled northeast across the far northwestern Atlantic and over the Labrador Sea. The emissions typically were lofted into the middle and upper troposphere along this path, with the ascent suspected to be most commonly due to WCBs. Once lofted, the trajectories generally entered the Arctic in a

region extending between western Nunavut, Canada and central Greenland. Similar to results for Asian anthropogenic emissions, trajectories that originated in the higher latitudes of North America typically entered the Arctic in the middle troposphere, while emissions from lower latitudes more frequently arrived in the upper troposphere.

Anthropogenic emissions from Europe were sampled along leg 8 of flight 8 on 12 April 2008. This conclusion is based on several factors. The purely anthropogenic tracer C_2Cl_4 was enhanced along this leg. High correlations between CH_4 , C_2H_6 , and C_3H_8 suggested an influence from natural gas emissions. These natural gas tracers were also well correlated with the purely anthropogenic tracer C_2Cl_4 . Similarly, enhanced mixing ratios of C_2H_2 and C_6H_6 also were found along leg 8, and since they were well correlated with C_2Cl_4 , they were determined to have been from anthropogenic sources as opposed to biomass burning.

Backward trajectories released along leg 8 indicated that the sampled air had passed within the boundary layer over eastern and western Europe. These are areas shown to have enhancements in anthropogenic emissions (Fig. 2f). Although WCBs seldom begin over Europe, a WCB was found to be responsible for the trajectories' ascent from the lower to the upper troposphere where they were sampled by the DC-8.

Much like the Asian and North American cases, the pathway and arrival altitude of emissions for the European case study were consistent with those for the entire ARCTAS-A period. European anthropogenic frequently traveled northward out of Europe, entering the Arctic across northern Europe and northeastern Russia. Although this scenario was the most common method by which trajectories reached the Arctic, some emissions, including those from our case study, traveled eastward between 50-70°N to wide range of Arctic entry locations along 70°N. Unlike the Asian and North American domains, emissions that originated in the higher latitudes of Europe more frequently entered the Arctic in the lower troposphere, while emissions originating further south arrived in the middle and upper troposphere.

Although biomass burning emissions dominated Arctic transport during ARCTAS-A (e.g., Warneke et al., 2009; Jacob et al., 2010), the current results emphasize that the historically important anthropogenic emissions cannot be neglected. However, in the future, biomass burning may become the dominant source of Arctic pollution due to increasing global temperatures that will promote enhanced numbers of wildfires (i.e., Kasischke et al., 2005).

REFERENCES

- Aucott, M. L., McCulloch, A., Graedel, T. E., Kleiman, G., Midgley, P., and Yi-Fan Li: Anthropogenic emissions of trichloromethane (chloroform, CHCl_3) and chlorodifluoromethane (HCFC-22): Reactive Chlorine Emissions Inventory, *J. Geophys. Res.*, 104, 8405-8415, 1999.
- Barletta B., Meinardi, S., Simpson, I. J., Atlas, E. L., Beyersdorf, A. J., Baker, A. K., Blake, N. J., Yang, M., Midyett, J. R., Novak, B. J., McKeachie, R. J., Fuelberg, H. E., Sachse, G. W., Avery, M. A., Campos, T., Weinheimer, A. J., Rowland, F. S., Blake, D. R.: Characterization of volatile organic compounds (VOCs) in Asian and north American pollution plumes during INTEx-B: Identification of specific Chinese air mass tracers, *Atmos. Chem. Phys.*, 9, 5371-5388, 2009.
- Barrie, L. A. and Hoff, R. M.: Five years of air chemistry observations in the Canadian Arctic, *Atmos. Environ.*, 19, 1995–2010, 1985.
- Barrie, L. A., Bottenheim, J. W., and Hart, W. R.: Polar Sunrise Experiment 1992 (PSE 1992): Preface, *J. Geophys. Res.*, 99, 25313–25314, 1994.
- Blake, N. J., Blake, D. R., Simpson, I. J., Meinardi, S., Swanson, A. L., Lopez, J. P., Katzenstein, A. S., Barletta, B., Shirai, T., Atlas, E., Sachse, G., Avery, M., Vay, S., Fuelberg, H. E., Kiley, C. M., Kita, K., Rowland, F. S.: NMHCs and halocarbons in Asian continental outflow during the Transport and Chemical Evolution over the Pacific (TRACE-P) Field Campaign: Comparison With PEM-West B, *J. Geophys. Res.*, 108(D20), 8806, doi:10.1029/2002JD003367, 2003.
- Blake, N. J., Streets, D. G., Woo, J., Simpson, I. J., Green, J., Meinardi, S., Kita, K., Atlas, E., Fuelberg, H. E., Sachse, G., Avery, M. A., Vay, S. A., Talbot, R. W., Dibb, J. E., Bandy, A. R., Thornton, D. C., Rowland, F. S., Blake, D. R.: Carbonyl sulfide and carbon disulfide: Large-scale distributions over the western Pacific and emissions from Asia during TRACE-P, *J. Geophys. Res.*, 109, D15S05, doi:10.1029/2003JD004259, 2004.
- Blake, D.: Whole air sampling (WAS) from the DC-8 aircraft during ARCTAS, 2008, available at: <http://www.espo.nasa.gov/arctas/docs/instruments/was.pdf>, 2008.
- Bradley, R.S., Keiming, F.T., and Diaz, H.F.: Climatology of surface-based inversions in the North American Arctic, *J. Geophys. Res.*, 97, 15,699-15,712, 1992.
- Butler, J. H., Montzka, S. A., Clarke, A. D., Lobert, J. M., and Elkins, J. W.: Growth and distribution of halons in the atmosphere, *J. Geophys. Res.*, 103(D1), 1503–1511, 1998.
- Carlson, T.N.: Speculations on the movement of polluted air to the Arctic, *Atmos. Environ.*, 15, 1473-1477, 1981.
- Carter, W. P. L.: Development of ozone reactivities for volatile organic compounds. *JAPCA J. Air Waste Ma.* 44, 881–899, 1994.

- Curry, J.A.: On the formation of continental polar air. *J. Atmos. Sci.*, 40, 2279-2292, 1983.
- Curry, J.A.: The contribution of radiative cooling to the formation of cold-core anticyclone, *J. Atmos. Sci.*, 44, 2575-2592, 1987.
- Ding, A., Wang, T., Xue, L., Gao, J., Stohl, A., Lei, H., Jin, D., Ren, Y., Wang, X., Wei, X., Qi, Y., Liu, J., Zhang, X.: Transport of north China air pollution by midlatitude cyclones: Case study of aircraft measurements in summer 2007, *J. Geophys. Res.*, 114, D08304, doi:10.1029/2008JD011023, 2009.
- Eckhardt, S., Stohl, A., Beirle, S., Spichtinger, N., James, P., Forster, C., Junker, C., Wagner, T., Platt, U., and Jennings, S.G.: The North Atlantic Oscillation controls air pollution transport to the Arctic. *Atmos. Chem. Phys.*, 3, 1769-1778, 2003.
- Eckhardt, S., Stohl, A., Wernli, H., James, P., Forster, C., and Spichtinger, N.: A 15-year climatology of warm conveyor belts, *J. Climate*, 17, 218-237, 2004.
- Fraser, P. J., Oram, D. E., Reeves, C. E., Penkett, S. A., and McCulloch, A.: Southern hemispheric halon trends (1978-1998) and global halon emissions, *J. Geophys. Res.*, 104(D13), 15985–16000, 1999.
- Fuelberg, H. E., Loring, Jr., R. O., Watson, M. V., Sinha, M. C., Pickering, K. E., Thompson, A. M., Sachse, G. W., Blake, D. R., and Schoeberl, M. R.: TRACE-A trajectory intercomparison 2. Isentropic and kinematic methods, *J. Geophys. Res.*, 101, 23927–23939, 1996.
- Fuelberg, H. E., Hannan, J. R., van Velthoven, P. F. J., Browell, E. V., Bieberbach, Jr., G., Knabb, R. D., Gregory, G. L., Pickering, K. E., and Selkirk, H. B.: A meteorological overview of the SONEX period, *J. Geophys. Res.*, 105, 3633–3651, 2000.
- Fuelberg, H. E., Harrigan, D. L., Sessions, W.: A meteorological overview of the ARCTAS 2008 mission, *Atmos. Chem. Phys.*, 10, 817-842, 2010.
- Hileman, B.: Arctic Haze, *Environ. Sci. Technol.*, 17(6), 232-236, doi:10.1021/es00112a602, 1983.
- Hoff, R. M.: Vertical structure of Arctic Haze observed by lidar, *J. Appl. Meteorol.*, 27, 125-139, 1987.
- Iverson, T.: On the atmospheric transport of pollution to the Arctic, *Geophys. Res. Lett.*, 11, 457-460, 1984.
- Jacob, D.J., Crawford, J. H., Maring, H., Clarke, A. D., Dibb, J. E., Emmons, L. K., Ferrare, R. A., Hostetler, C. A., Russell, P. B., Singh, H. B., Thompson, A. M., Shaw, G. E., McCauley, E., Pederson, J. R., Fisher, J. A.: The Arctic Research of the Composition of the Troposphere from Aircraft and Satellites (ARCTAS) mission: Design, execution and first results, *Atmos. Chem. Phys.*, 10, 5191-5212, 2010.

- Kasischke, E. S., Hyer, E. J., Novelli, P. C., Bruhwiler, L. P., French, N. H. F., Sukhinin, A. I., Hewson, J. H., and Stocks, B. J.: Influences of boreal fire emissions on Northern Hemisphere atmospheric carbon and carbon monoxide, *Global Biogeochem. Cy.*, 19, GB1012, doi:10.1029/2004GB002300, 2005.
- Katzenstein, A. S., Doezeema, L. A., Simpson, I. J., Blake, D. R., and Rowland, F. S.: Extensive regional atmospheric hydrocarbon pollution in the southwestern United States, *Proc. Nat. Acad. Sciences*, 100, 11, 975-11, 979, 2003.
- Kettle, A. J., Kuhn, U., von Hobe, M., Kesselmeier, J., Andreae, M. O.: Global budget of carbonyl sulfide: Temporal and spatial variations of the dominant sources and sinks, *J. Geophys. Res.*, 107(D22), 4658, doi:10.1029/2002JD002187, 2002.
- Klonecki, A., Hess, P., Emmons, L., Smith, L., and Orlando, J.: Seasonal changes in the transport of pollutants into the Arctic troposphere-model study, *J. Geophys. Res.*, 8367, doi:1029/2002JD002199, 2003.
- Law, K. S. and Stohl, A.: Arctic air pollution: Origins and impacts, *Science*, 315, 1537-1540, doi: 10.1126/science.1137695, 2007.
- Lee, B. H., Munger, J. W., Wofsy, S. C., and Goldstein, A. H.: Anthropogenic emissions of nonmethane hydrocarbons in the northeastern United States: Measured seasonal variations from 1992–1996 and 1999–2001, *J. Geophys. Res.*, 111, D20307, doi:10.1029/2005JD006172, 2006.
- Li, S. M. and Barrie, L. A.: Biogenic sulphur aerosols in the Arctic troposphere. 1. Contributions to sulphate. *J. Geophys. Res.* 98D, 20, 613–20 622, 1993.
- Martin, B. D., Fuelberg, H. E., Blake, N. J., Crawford, J. H., Logan, J. A., Blake, D. R., and Sachse, G. W.: Long range transport of Asian outflow to the equatorial Pacific, *J. Geophys. Res.*, 108(D2), 8322, doi:10.1029/2001JD001418, 2002.
- Matsui, H., Kondo, Y., Moteki, N., Takegawa, N., Sahu, L. K., Zhao, Y., Fuelberg, H. E., Sessions, W., Diskin, G., Blake, D. R., and Whithaler, A.: Seasonal variation of the transport of black carbon aerosol from the Asian continent to the Arctic during the ARCTAS aircraft campaign, Submitted to *J. Geophys. Res.*, 2010.
- Meyer, F. G., Curry, J. A., Brock, C. A., Radke, L. F.: Springtime visibility in the Arctic, *J. Appl. Meteorol.*, 30, 342-357, 1990.
- Mitchell, J. M. Jr.: Visual range in the polar regions with particular reference to the Alaskan Arctic, *J. Clim. Appl. Meteorol.*, 23, 916-928, 1957.
- Montzka, S. A., Hall, B. D., Elkins, J. A.: Accelerated increases observed for hydrochlorofluorocarbons since 2004 in the global atmosphere, *Geophys. Res. Lett.*, 36, L03804, doi:10.1029/2008GL036475, 2009.

Oltmans, S. J., Lefohn, A. S., Harris, J. M., Tarasick, D. W., Thompson, A. M., Wernli, H., Johnson, B. J., Davies, J., Novelli, P. C., Montzka, S. A., Sweeney, C., Patrick, L. A., Jefferson, A., Dann, T., Ray, J. D., Shapiro, M.: Enhanced ozone over western North America from biomass burning in Eurasia during April 2008 as seen in surface and profile observations, Submitted to Atmos. Environ., 2010.

Products on the NCEP FTP Server: <http://www.nco.ncep.noaa.gov/pmb/products/>, access 15 July 2010.

Quinn, P. K., Miller, T. L., Bates, T. S., Ogren, J. A., Andrews, E., Shaw, G. E.: A three-year record of simultaneously measured aerosol chemical and optical properties at Barrow, Alaska. *J. Geophys. Res.*, 107(D11), 10.1029/2001JD001248, 2002.

Raatz, W. E. and Shaw, G. E.: Long-range tropospheric transport of pollution aerosols in the Alaskan Arctic, *J. Clim. Appl. Meteorol.*, 23, 1052–1064, 1984.

Raatz, W. E.: The climatology and meteorology of Arctic air pollution, in: *Pollution of the Arctic Atmosphere*, edited by W.T. Sturges, Elsevier, New York, 13-42, 1991.

Reid, J., Hyer, E. J., Prins, E. M., Westphal, D. L., Zhang, J., Wang, J., Christopher, S. A., Curtis, C. A., Schmidt, C. A., Eleuterio, D. P., Richardson, K. A., and Hoffman, J. P.: Global Monitoring and Forecasting of Biomass Burning Smoke: Description of and Lessons From the Fire Locating and Modeling of Burning Emissions (FLAMBE) Program, *IEEE J. Sel. Top. Appl.*, 2, 2009.

Rinke, A., Dethloff, K., and Fortmann, M.: Regional climate effects of Arctic Haze, *Geophys. Res. Lett.*, 31, L16202, 2004.

Russo, R., Talbot, R. W., Dibb, J. E., Scheuer, E., Seid, G., Jordan, C. E., Fuelberg, H. E., Sachse, G. W., Avery, M. A., Vay, S. A., Blake, D. R., Blake, N. J., Atlas, E., Fried, A., Sandholm, S. T., Tan, D., Singh, H. B., Snow, J., Heikes, B. G.: Chemical composition of Asian continental outflow over the western Pacific: Results from Transport and Chemical Evolution over the Pacific (TRACE-P), *J. Geophys. Res.*, 108(D20), 8804, doi:10.1029/2002JD003184, 2003.

Russo, R. S., Zhou, Y., White, M. L., Mao, H., Talbot, and Sive, B. C.: Multi-year (2004-2008) record of nonmethane hydrocarbons and halocarbons in New England: seasonal variations and regional sources, *Atmos. Chem. Phys.*, 10, 4909-4929, 2010.

Schnell, R. C.: Arctic haze and the Arctic gas aerosol sampling program (AGASP), *Geophys. Res. Lett.*, 11, 361-364, 1984.

Shaw, G. E.: The Arctic haze phenomenon, *B. Am. Meteorol. Soc.*, 76, 2403-2413, 1995.

Shaw, G. E.: Evidence for a central Eurasian source area of Arctic haze in Alaska, *Nature*, 299, 815-818, 1982.

Simpson, I. J., Meinardi, S., Blake, N. J., Rowland, F. S., and Blake, D. R.: Long-term decrease in the global atmospheric burden of tetrachloroethene (C_2Cl_4), *Geophys. Res. Lett.*, doi:10.1029/2003GL019351, 2004.

Simpson, I. J., Blake, N. J., Barletta, B., Diskin, G. S., Fuelberg, H. E., Gorham, K., Huey, L. G., Meinardi, S., Rowland, F. S., Vay, S. A., Weinheimer, A. J., Yang, M., Blake, D. R.: Characterization of trace gases measured over Alberta oil sands mining operations: 76 speciated C_2 - C_{10} volatile organic compounds (VOCs), CO_2 , CH_4 , CO , NO , NO_2 , NO_y , O_3 and SO_2 , Submitted to *Atmos. Chem. Phys.*, 2010.

Singh, H. B., Anderson, B. E., Brune, W. H., Cai, C., Crawford, J. H., Cohen, R. C., Czech, E. P., Emmons, L., Fuelberg, H. E., Huey, G., Jacob, D. J., Jimenez, J. L., Kondo, Y., Kaduwela, A., Mao, J., Olson, J. R., Sachse, G. W., Vay, S. A., Weinheimer, A., Wennberg, P. O., Wisthaler, A.: Pollution influences on atmospheric composition and chemistry at high northern latitudes: Boreal and California forest fire emissions, *Atmos. Environ.*, 44, 4553-4564, 2010.

Skamarock, W. C., Klemp, J. B., Dudhia, J., Gill, D. O. Barker, D. M., Duda, M. G., Huang, X., Wang, W., and Powers, J. G.: A description of the Advanced Research WRF version 3. NCAR Tech. Note NCAR/TN-475+STR, 113 pp., 2008.

Stohl, A., Wotawa, G., Seibert, P., and Kromp-Kolb, H.: Interpolation errors in wind fields as a function of spatial and temporal resolution and their impact on different types of kinematic trajectories, *J. Appl. Meteorol.*, 34, 2149–2165, 1995.

Stohl, A., Hittenberger, M., and Wotawa, B.: Validation of the Lagrangian particle dispersion model FLEXPART against large scale tracer experiments, *Atmos. Environ.*, 32, 4245–4264, 1998.

Stohl, A.: A 1-year lagrangian “climatology” of airstreams in the Northern Hemisphere troposphere and lowermost stratosphere, *J. Geophys. Res.*, 106(D7), 7263-7279, 2001.

Stohl, A., Eckhardt, S., Forster, C., James, P., Spichtinger, N.: On the pathways and timescales of intercontinental air pollution transport, *J. Geophys. Res.* 107(D23), 4684, doi:10.1029/2001JD001396, 2002.

Stohl, A.: Characteristics of atmospheric transport into the Arctic troposphere, *J. Geophys. Res.*, D11306, doi:1029/2005JD006888, 2006.

Stohl, A. and Law, K.: IGACtivities Newsletter, available online at: http://www.igac.noaa.gov/newsletter/igac33/May_2006_IGAC_33.pdf, 33, 16–32, 2006.

Streets, D. G., Bond, T. C., Carmichael, G. R., Fernandes, S. D., Fu, Q., He, D., Klimont, Z., Nelson, S. M., Tsai, N. Y., Wang, M. Q., Woo, J. H., and Yarber, K. F.: An inventory of gaseous and primary aerosol emissions in Asia in the year 2000, *J. Geophys. Res.*, 108(D21), 8809, doi:10.1029/2002JD003093, 2003.

Warneke, C., McKeen, S. A., de Gouw, J. A., Goldan, P. D., Kuster, W. C., Holloway, J. S., Williams, E. J., Lerner, B. M., Parrish, D. D., Trainer, M., Fehsenfeld, F. C., Kato, S., Atlas, E. L., Baker, A., Blake, D. R.: Determination of urban volatile organic compound emission ratios and comparison with an emissions database, *J. Geophys. Res.*, 112, D10S47, doi:10.1029/2006JD007930, 2007.

Warneke, C., Bahreini, R., Brioude, J., Brock, C. A., de Gouw, J. A., Fahey, D. W., Froyd, K. D., Holloway, J. S., Middlebrook, A., Miller, L., Montzka, S., Murphy, D. M., Peischl, J., Ryerson, T. B., Schwarz, J. P., Spackman, J. R., Veres, P.: Biomass burning in Siberia and Kazakhstan as an important source for haze over the Alaskan Arctic in April 2008, *Geophys. Res. Lett.*, 36, L02813, doi:10.1029/2008GL036194, 2009.

Warneke, C., Froyd, K. D., Brioude, J., Bahreini, R., Brock, C. A., Cozic, J., de Gouw, J. A., Fahey, D. W., Ferrare, R., Holloway, J. S., Middlebrook, A. M., Miller, L., Montzka, S., Schwarz, J. P., Sodemann, H., Spackman, J. R., Stohl, A.: An important contribution to springtime Arctic aerosol from biomass burning in Russia, *Geophys. Res. Lett.*, 37, L01801, doi:10.1029/2009GL041816, 2010.

Watts, S. F.: The mass budget of carbonyl sulfide, dimethyl sulfide, carbon disulfide, and hydrogen sulfide, *Atmos. Environ.*, 34, 761-779, 2000.

Xiao, Y., Logan, J. A., Jacob, D. J., Hudman, R. C., Yantosca, R., and Blake, D. R.: Global budget of ethane and regional constraints on U.S. sources, *J. Geophys. Res.*, 113, D21306, doi:10.1029/2007JD009415, 2008.

BIOGRAPHICAL SKETCH

Donal Harrigan was born in Miami, FL on May 16, 1984. Shortly after his birth, his family moved to central Florida where Donal lived until graduating high school. In 2002 Donal enrolled in college at the Florida Institute of Technology (FIT) in Melbourne, FL. Picking the major “Aviation Meteorology” was the easiest decision he made in his collegiate career. His father, an airline pilot and certifiable weather nut, was responsible for Donal’s interest in aviation and meteorology. Unfortunately, at the time Donal started college, his interest in the ocean, surfing, and other non FIT sanctioned activities, far outweighed his interest in school. Once his family realized that they were going to have to fund more than 4 years at a private institution, Donal enrolled at FSU to continue his meteorology degree.

With a new attitude toward school, Donal succeeded in earning a bachelor’s degree in meteorology. During his time as an undergraduate student, Donal worked at WTXL, the local ABC affiliate as the weekend meteorologist. He quickly learned that this was not the direction he wanted to continue in with his career. After graduating, he left his job in television, applied and was granted admission to the graduate program at FSU. The importance of a higher education was made clear to Donal at an early age; his father earned a bachelor’s degree, his mother a master’s degree, and his sister a PhD. Once in the masters program, Donal received a highly competitive position with the National Weather Service (NWS) as a SCEP intern.

Upon graduation, Donal hopes to remain in Florida, with his fiancée Sarah, where they can be near both of their families. Donal hopes to have a long career with the NWS following his passion of operational meteorology and would like to continue doing research that applies to his field.